A TIME-VARYING SUBSIDENCE PARAMETERIZATION FOR THE ATMOSPHERIC BOUNDARY LAYER

BY

DAVID D. FLAGG

SUBMITTED TO THE DEPARTMENT OF EARTH, ATMOSPHERIC AND PLANETARY SCIENCES IN PARTIAL FULFILLMENT OF THE REQUIREMENTS FOR THE DEGREE OF

MASTER OF SCIENCE

AT THE

MASSACHUSETTS INSTITUTE OF TECHNOLOGY

JUNE 2005

Author:_____

Department of Earth, Atmospheric and Planetary Sciences
May 6, 2005

Certified by:_____

Dara Entekhabi
Professor
Thesis Supervisor

Accepted by:_____

Maria T. Zuber
E.A. Griswold Professor of Geophysics and Planetary Science
Department Head

ABSTRACT

This study examines the effect of a time-varying parameterization for subsidence in the atmospheric boundary layer (ABL) on a one-dimensional coupled land-atmosphere model. Measurements of large-scale divergence in the ABL are scarce and often marred by error, providing the motivation to model this important physical process and estimate its values from indirect but related observations. Constant parameterizations of large-scale divergence and/or subsidence velocity are adequate for periods within a characteristic synoptic time scale, but longer studies require a parameterization that yields to local atmospheric change. After confirming the potential significance of subsidence in the ABL, this experiment investigates two key areas: (1) the ability to model subsidence change as a response to estimated time-varying model error and (2) the net improvement and potential benefits of this enhancement. This study indicates a consistent reduction of root-mean-square error scores for the time-varying subsidence (divergence) parameter scheme versus a constant parameterization for the 2 m specific humidity measurement, with negligible change to the 2 m temperature measurement. Model error does not improve explicitly, in spite of the presumed improvement to model physics. However, the unknown nature of the model error precludes an accurate diagnose of change, thus leaving the root-mean-square-error scores as the principal tool of evaluation and hence the justifying the potential usefulness of the time-varying parameterization.

1. INTRODUCTION

From the linearized form of the vertical component of the conservation of momentum for turbulent flow under the Boussinesq approximation,

$$\frac{d(\overline{w}+w')}{dt} = -\frac{\rho'}{\overline{\rho}}g - \frac{1}{\overline{\rho}}\frac{\partial p'}{\partial z} + \nu_m \frac{\partial^2(\overline{w}+w')}{\partial x_j^2} \qquad (1),$$

the linearly averaged vertical velocity, ($\overline{w}$), is frequently defined as subsidence[1]. It plays a minimal role in the momentum equation because it rarely exceeds 0.1 ms^{-1}, whereas vertical velocity fluctuations (w') can vary up to 5 ms^{-1} (Stull 1988). However, subsidence can have a significant influence on mass conservation, mixed layer growth and particulate dispersion in the atmospheric boundary layer (ABL). The important potential influence of subsidence on ABL dynamics is well documented (Stull 1988, Sempreviva and Gryning 2000, Yi et al. 2001). Being a linearly averaged velocity, it represents the mean rate of divergence in the ABL and is governed principally by synoptic-scale weather. Measurement of this low-magnitude velocity is particularly difficult by plane due to the corrupting velocity bias and by in-situ observation because of background noise in the signal. Consequently, when modeling the ABL, subsidence is often solved from divergence estimates, parameterized or neglected all together.

Subsidence receives varied treatment among ABL models. A scarcity of divergence measurements typically forces parameterization. The parameterization differs for models based on a turbulent kinetic energy budget (Driedonks 1982, Driedonks and Tennekes 1984) versus slab ABL models (Steyn and Oke 1982, Batchvarova and Gryning 1994, Ek and Mahrt 1994). In some cases, subsidence is explicitly neglected (De Ridder 1997, McNaughton and Spriggs 1986, ME04), deemed negligible (Batchvarova et al. 1999, 2001) or implicitly included as part of a forcing residual (Fitzjarrald 1982, Sorbjan 1995). The most widely documented technique involves parameterization in a slab ABL model. In that case, subsidence is parameterized as a velocity and is incorporated into prognostic governing equations.

[1] Note that the velocity qualifier, 'subsidence,' denotes that the vertical velocity is negative. When used alone, 'subsidence' itself refers to any condition of negative vertical velocity. The terms subsidence and subsidence velocity are often used interchangeably.

Stull (1973) provides an early reference to the parameterization of subsidence as a velocity. The vertical gradient of the subsidence velocity is solved by arguments of continuity in the troposphere, given by:

$$\frac{\partial w_L}{\partial z} = -\left(\frac{\partial u}{\partial x} + \frac{\partial v}{\partial y}\right) \qquad (2),$$

where Stull (1973) calls w_L the vertical wind velocity. Assuming that the large-scale divergence (RHS of (2)) can be described by a constant, b, integration of (2) gives the large-scale, mean vertical wind velocity (i.e., subsidence velocity) at height (z) :

$$w_L = -bz \qquad (3).$$

Steyn and Oke (1982) incorporate (3) into their mixed layer model, defining a subsidence parameter (β) in place of (b). The process of subsidence enters the model when describing its effects on air parcels in a Lagrangian frame. The total change in the height of an air parcel owing to large-scale subsidence over a defined time period is used in conjunction with the mixed layer lapse rate and initial-time parcel potential temperature to solve the final time parcel potential temperature. Thus, subsidence enters the model through changes to potential temperature.

Stull (1976) offers a different approach by incorporating (3) into a mixed layer depth prognostic equation. The large-scale subsidence velocity, combined with the "cloud-induced subsidence" velocity (Stull 1976) and entrainment velocity, defines the total time rate change of the mixed layer depth. The strategy of incorporating subsidence velocity through the ABL height or mixed layer depth prognostic equation is repeated in successive studies (Deardorff and Peterson (1980), Batchvarova and Gryning (1994), Sempreviva and Gryning (2000)). McNaughton and Spriggs (1986) and Margulis and Entekhabi (2004) offer further support for the approach. Although both studies explicitly neglect subsidence in their mixed layer model, both suggest the potential benefits of the incorporation of a subsidence velocity in the mixed layer depth prognostic equation.

It is clear that several methods exist for parameterizing subsidence in the ABL. However, it is apparent that incorporating subsidence through an ABL height or mixed

layer depth prognostic equation is a commonly accepted and thoroughly tested method. For this reason, the mixed layer depth approach to subsidence inclusion is selected for use in this study.

Given its limited magnitude with respect to perturbation vertical velocity, a highly pertinent question to ask is: Why is it necessary to incorporate a subsidence velocity into a model of the ABL? One key reason, especially pertinent to one-dimensional coupled land-ABL models, is its role in mass conservation. In the absence of an explicit solution to advection, subsidence (based on a measured divergence rate or well-estimated b value) may provide the only representation of mass continuity changes in the atmospheric column. A more general reason applicable to all ABL models is its non-negligible effect on principal ABL state variables and processes. Such key terms include mean ABL potential temperature (θ), mean ABL specific humidity (q), entrainment, mixed layer depth (h), and surface fluxes of sensible heat and latent heat. As will be shown in Section 5, these effects can be significant, amounting to a five to ten percent change in h, for example. These changes have potential implications in multiple-day ABL studies such as aerosol dispersion (De Wekker et al. 2004, Price et al. 2004) and CO_2 fluxes (de Arellano et al. 2004) where inadequate subsidence parameterization may unfairly bias any sensitive chemistry.

One trait common to studies incorporating subsidence into ABL models, including those described above, is a constant subsidence parameter (e.g., b or β). For studies of daytime or noctural ABL dynamics (or even periods of a few days or less), this method is practical given a reliable estimate of b. However, many of the recent ABL studies referenced above focus on long-term (multiple day) evolution of chemistry. Given the potential implications of subsidence on mixed-layer depth, temperature and moisture, all crucial components in aerosol dispersion, it is necessary to implement a subsidence estimation process that will be valid for long-term model integrations. Moreover, because subsidence in the ABL is governed by synoptic cycles (roughly four days in the mid-latitudes), it makes sense to evaluate subsidence and its influence on a similar time scale. Building on the effects resolved by a constant parameterization (3), this study seeks to permit long-term ABL study by creating a time-varying subsidence parameterization.

This study evaluates the viability and net effects of a time-varying subsidence parameterization on a 1-D coupled land-ABL model (Margulis and Entekhabi 2001, hereafter ME01) without the constraint of additional observation. It will verify that this parameterization improves model performance. The model, discussed in Section 4, is solved by a variational approach where misfit of model estimates and assimilated data drive a separate adjoint model which seeks to minimize initial value error through an iterative process. Model improvement is the principal gage for viability, measured by a reduction in the root-mean-square error (RMSE) score of the model-measurement misfit. Viability tests also examine changes to model error (representing missing model physics) owing to the inclusion of subsidence. To diagnose the net effects of the parameterization, this study enumerates the change to principal ABL state variables and fluxes. Additional sensitivity tests are conducted to enhance understanding of the effects on the model.

Section 2 of this study examines the analytical effects of subsidence on the ABL to better understand how this process will affect the model. Section 3 will outline the design of the study including the tests and the relevance of the experiment. In Section 4, the model and its components are described. Section 5 presents the experimental results, which are analyzed in Section 6. Section 7 offers potential applications and future directions for this work as well as a review of key limitations. This is followed by conclusions in Section 8.

2. THEORY: THE EFFECT OF SUBSIDENCE ON THE MIXED LAYER

The analytical effect of subsidence on the mixed layer can be discerned qualitatively by examining a closed first order set of governing equations for a slab ABL (equations 4-10). Closure here is obtained by parameterizing the entrainment velocity (w_e, (6a)). All remaining unknowns not explicitly solved here are specified (such as c_h, γ_θ and γ_q) or estimated internally (such as G_*, H_c and E_{top}). All symbols and abbreviations are listed in Appendix A.

Mixed layer energy and moisture budgets:

$$\rho c_p h \frac{d\theta}{dt} = (R_{ad} + R_{cu} + R_{gu})\varepsilon_a - R_{Ad} - R_{Au} + H_c + H_g + H_{top} \tag{4}$$

$$\rho h \frac{dq}{dt} = E_c + E_g + E_{top} \tag{5}$$

Mixed layer depth:

$$\frac{dh}{dt} = w_e + w_L \tag{6}$$

$$w_e = \frac{2\theta G_* \mathbf{exp}(-\xi h)}{gh\delta_\theta} + c_h \frac{H_v}{\rho c_p \delta_\theta} \tag{6a}$$

Sensible Heat and Dry Air Entrainment:

$$H_{top} = \rho c_p \delta_\theta w_e \tag{7}$$

$$E_{top} = \rho \delta_q w_e \tag{8}$$

Inversion strength:

$$\frac{d\delta_\theta}{dt} = \gamma_\theta w_e - \frac{d\theta}{dt} \tag{9}$$

$$\frac{d\delta_q}{dt} = \gamma_q w_e - \frac{dq}{dt} \tag{10}$$

.

a. *Effect of subsidence on entrainment and inversion strength*

To understand the effect of subsidence on entrainment, it is necessary to evaluate the physical changes to θ, q, δ_θ, δ_q and w_e through a parametric approach assuming fair weather conditions. The incorporation of a large-scale, negative vertical velocity, w_L, (a.k.a. subsidence) in (6) serves to reduce the rate of mixed layer growth from the value determined by the entrainment velocity, w_e, alone. The reduced mixed layer

depth increases the magnitude of $\frac{d\theta}{dt}$ and $\frac{dq}{dt}$ by (4) and (5), respectively. During mixed layer growth, the heat fluxes H_c, H_g, E_c, E_g and H_{top} are all positive. Thus, $\frac{d\theta}{dt}$ must sustain a net increase (i.e., net ABL warming). For $\frac{dq}{dt}$, however, because the jump in the specific humidity profile across the entrainment layer, δ_q, is generally negative for daytime conditions, E_{top} is also negative by construction in (8). Typically, the magnitude of the dry air entrainment flux will exceed the surface fluxes (E_c and E_g). Following the late-afternoon collapse of the ABL, entrainment fluxes gradually vanish, while surface fluxes diminsh to nearly zero. Therefore, it is expected that, in fair weather, the increase in the magnitude of $\frac{dq}{dt}$ due to reduced h provides a net decrease of $\frac{dq}{dt}$ and thus promotes net ABL drying[2]. At night, in the absence of entrainment and radiative fluxes, surface fluxes will dictate the heat and moisture changes in the mixed layer. A discussion of these fluxes follows in Section 2.c.

The two remaining terms that determine net change to the inversion prognostic equations (9 and 10), which are required to find the net effect of subsidence on entrainment, are the entrainment velocity (w_e) and free-atmosphere lapse rates (γ_θ and γ_q). The net h decrease and net $\frac{d\theta}{dt}$ increase augment w_e (6a). However, the net warming has a detrimental effect on surface sensible heat flux (see Section 2.a.iii), a major component of the free convection term of (6a). Assuming a typical mid-latitude, fair weather subsidence velocity (1 cm s^{-1}), the net (positive) h reduction and θ warming components outweigh the net (negative) surface sensible heat flux, giving a net increase of w_e. The free atmosphere lapse rates of θ and q (γ_θ and γ_q, respectively) are best-fit quadratic equations and must be derived with coefficients to

---

[2] Note that if weather conditions are not fair or if precipitation is imminent, then $\frac{dq}{dt}$ may be greater than zero. In this case, h-reduction will serve to increase $\frac{dq}{dt}$.

allow the updated h values to fit with radiosondes observations of θ and q. They are exempt from influence by subsidence inclusion. Thus, subsidence should provoke net increase of w_e.

Consequently, by (10), net ABL drying promotes increasing $\frac{d\delta_q}{dt}$ while the net w_e enhancement promotes decreasing $\frac{d\delta_q}{dt}$. Order of magnitude estimates suggest the net drying as dominant. Therefore, $\frac{d\delta_q}{dt}$ sustains a net increase during the day, when E_{top} governs $\frac{dq}{dt}$, thus weakening the q inversion. At night, when E_c and E_g are left to sustain $\frac{dq}{dt}$, $\frac{d\delta_q}{dt}$ sustains a slight net decrease. The net effect of subsidence on $\frac{d\delta_\theta}{dt}$ is more nebulous. Both RHS terms of (9) sustain a net increase and are positive values. Order of magnitude estimates suggest that changes to the second term dominate during the day, thus leading to a net daytime decrease in $\frac{d\delta_\theta}{dt}$, hence weakening the θ inversion. It is therefore apparent that subsidence has the net effect of weakening both the q and θ inversions.

The final step in determining the effect of subsidence on entrainment is to apply the changes in δ_θ, δ_q and w_e to (7) and (8). The net effect of subsidence on H_{top} should vary according to the time of day. Prior to sunrise, the net cooling from surface fluxes creates a temporarily enhanced inversion (net $\delta_\theta > 0$). Thus, given that net $w_e > 0$, net H_{top} is initially positive by (7), enhancing sensible heat entrainment. However, as the mixed layer grows, the subsidence velocity increases, quickly substituting a net warming in the mixed layer, as described above[3]. This net warming diminishes the inversion strength. When the net change to δ_θ turns negative, net H_{top} must also turn negative, reducing sensible heat entrainment. In the afternoon, the net warming continues, but the net w_e should gradually wane due to the net reduction of surface

[3] Note, also, that the initially net positive H_{top} will accelerate the warming of the mixed layer.

sensible heat fluxes (see Section 2.c). Thus, though net H_{top} should turn negative during the day, the difference should not be substantial.

The influence of subsidence on E_{top} is similarly delicate. There is an expected daytime net increase in δ_q (e.g., less negative, hence, weakened inversion), coupled with a ubiquitously positive net change to w_e. Order of magnitude estimates show that the latter net changes outweigh the former, thus giving a net negative E_{top}, enhancing dry air entrainment. Therefore, it is concluded that daytime subsidence has a generally negative effect on sensible heat entrainment (net ABL cooling) and a consistently positive effect on dry air entrainment (net ABL drying). At night, subsidence will likely produce reversed results, but on a much smaller magnitude due to the relatively weak surface fluxes, with the exception of the sensible heat budget near sunrise as described above.

b. *Effect of subsidence on mixed layer potential temperature and specific humidity*

From the results of Section 2.a, it is apparent that subsidence has varied effects on the terms comprising the mixed layer energy budget (4). Specifically, the net mixed layer cooling due to sensible heat entrainment reduction competes with the net mixed layer warming due to mixed layer depth reduction. Additionally, subsidence indirectly reduces surface sensible heat flux (Section 2.c.i), contributing to ABL cooling. However, the sensible heat entrainment reduction (Section 2.a) is limited to the daytime. Moreover, there are variations in the timing of the net effect on surface sensible heat fluxes, further complicating the net change in mixed layer θ. Therefore, although physical intuition suggests a net warming, analytical evidence portrays opposing forces on temperature. Numerical study is required to confirm a net warming.

Under fair weather conditions, the net enhancement to dry air entrainment and the net h reduction owing to subsidence both support a net drying of the mixed layer. However, surface fluxes support net moistening (Section 2.c.ii). At night, both the net entrainment and h reduction effects nearly vanish. The remaining, minimal overnight net h reduction will support a net moistening from surface fluxes (Section 2.c.ii), thus opening the possibility of a net nocturnal moistening from subsidence.

c. *Effect of subsidence on surface fluxes*

i. Surface Sensible Heat Flux

The effect of subsidence on surface fluxes appears to vacillate on a diurnal cycle. In the presence of mixed layer net warming, the surface-air temperature gradient weakens and, consequently, reduces the ground and canopy sensible heat fluxes, H_g and H_c. Given that subsidence velocity peaks in the late afternoon, the net warming due to h reduction peaks concurrently, minimizing the surface-air temperature gradient. Combined with a net H_{top} reduction (Section 2.a), these heat flux reductions act to counter a net warming. Note the dependence of surface heat flux reduction on the existence of a net warming to reduce the surface-air temperature gradient. Thus, in light of the uncertainty posed in Section 2.b with regard to the net effect of subsidence on ABL potential temperature, it is likely that changes to surface flux will not create a net ABL cooling but, rather, diminish any net warming. At night, sensible heat entrainment diminishes to nearly zero, leaving only surface fluxes to cool the mixed layer (given the presence of a net warming that reduces the surface-air temperature gradient). These nocturnal fluxes should be considerably smaller given the minimal h reduction by subsidence overnight. The net effect of subsidence on surface sensible heat flux, assuming a net mixed layer warming, is a reduction of the flux (and thus a net cooling), minimized overnight.

ii. Surface Latent Heat Flux

Given a net moistening of the mixed layer (Section 2.b), the ambient vapor pressure (e) increases. A net warming of the mixed layer may also translate into a net warming of near surface temperatures at the canopy (T_c) and ground levels (T_g). Thus, one may anticipate a net increase of the saturation vapor pressure at the canopy ($e_s(T_c)$) and ground ($e_s(T_g)$). The strength of the canopy (ground) latent heat flux derives principally from the discrepancy between e and $e_s(T_c)$ ($e_s(T_g)$). Therefore, because both the vapor pressure and saturation vapor pressures may increase due to the presence of subsidence, it is unclear from theory exactly how the strength of the surface latent heat flux will change. Such a determination requires numerical testing.

In terms of diurnal variation, because the net warming and net moistening are likely to wane in the nocturnal boundary layer, it is likely that the net change to the surface latent heat flux strength will similarly diminish.

3. APPROACH

a. Design

This study applies an ABL subsidence parameterization to a multiple-day setting. In the interest of focusing on the viability of the time-varying nature of the parameterization, the method follows that outlined by Stull (1973), Steyn and Oke (1982) and other subsequent studies referenced in Section 1.b. The large-scale subsidence velocity, hereinafter referred to as the subsidence velocity, w_L, is defined by (11). It is identical to (3) but with 'β_s 'as the subsidence parameter (a.k.a. ABL large scale divergence parameter, units of s^{-1}) so as to avoid confusion with other variables already defined in the numerical model. Note also that the mixed layer depth in (3), z, becomes h following the convention of the model in Section 2:

$$w_L = \beta_s h \qquad (11).$$

The negative sign in (3) is absorbed into β_s such that a negative value represents subsidence and a positive value implies large-scale ascent in the ABL.

Initial guess estimates of β_s are drawn from a range of values suggested by the literature for fair weather conditions. Table 1 depicts a range of estimates of the subsidence/divergence parameter, β_s, and/or subsidence velocity from selected ABL studies. The dataset used in conjunction with this study (Section 4.c) is generally void of precipitation, but a frontal passage halfway through the period provides a noticeable change in the local observations (Figure 2). Before and after this event, generally clear to fair skies and dry weather conditions dominate. In light of the variable presence of dry conditions and significant ABL divergence, initial β_s estimates are generally confined to the range $[-1.10\times10^{-5}\,s^{-1} \geq \beta_s \geq -0.40\times10^{-5}\,s^{-1}]$.

To make β_s time-varying, one can define a simple prognostic first-order ordinary differential equation (ODE) to describe its growth in time. This ODE and its operation are described in Section 4. In addition to defining the evolution of β_s, the model (its adjoint, specifically) also acts to revise the initial value of β_s (β_{s_0}) in an attempt to minimize the misfit between model estimates and the assimilated measurements. The measurements assimilated, also detailed in Section 4, include a 2 m temperature (T_r), 2 m specific humidity (q_r) and a surface temperature (T_s), all at a 30-minute sampling rate.

It is expected that the initial value estimation process, combined with the ODE, will allow a reasonable β_{s_0} estimate to produce a β_s time-series. When this time-series is applied to (11), it will properly diagnose the evolution of the subsidence velocity and, subsequently, correct model physics as expected from theory (Section 2). Of principal interest is how this process will improve model physics and model performance.

Source	Estimated Subsidence Velocities				Estimated Subsidence Parameter	Conditions and Remarks
	w_L (cm s^{-1})	β_s (x 10^{-5} s^{-1}) derived from w_L			β_s (x 10^{-5} s^{-1})	
		h = 0.5 km	h = 1.5 km	h = 2.5 km		
Letzel and Raasch (2002)	-2.00	-4.00	-1.33	-0.80		High pressure, clear skies
Sempreviva and Gryning (2000)	-1.20	-2.40	-0.80	-0.48		Magnitude of subsidence exceeds that of entrainment
Stevens et al. (2001)	-0.65	-1.30	-0.43	-0.26		Potentially cloud-topped ABL; authors believe w_L may be too small, set to create adequate cloud cover
Kirkpatrick et al. (2003)	-0.30	-0.60	-0.20	-0.12		Cloud-topped ABL
Stull (1976)					1.00	Minimal cloud cover, mid-latitudes
Stull (1976)					2.60	Minimal cloud cover, sub-tropics
Yi et al. (2000)	-1.85	-3.70	-1.23	-0.74		Average of 19 daily estimates over 7 months; all under high pressure, clear skies, minimal horizontal wind
Carlson and Stull (1986)	-2.25	-4.50	-1.50	-0.90	1.63	Average of 8 nocturnal estimates taken over five days, fair weather

Table 1: A comparison of subsidence parameterizations from clear and cloudy sky ABL studies, including constant subsidence velocity schemes (left column) and constant subsidence / divergence parameters (right column). Note that the subsidence parameters listed to the right of the subsidence velocities are derived by plugging the velocity into (11), to allow comparison with right column data.

b. Experiments

An array of test cases will consider these two issues by comparing results from three model cases: '*sub*' (time-varying β_s parameterization), '*sub constant*' (a constant β_s parameterization) and '*nosub*' (void of any subsidence accounting method). These three cases are also listed in Table 2 for reference.

Case Title	Method of Subsidence Parameterization
sub	β_s varies in time; β_s evolves according to (14)
sub constant	β_s is constant ($\beta_s = 0.60 \times 10^{-5}\ s^{-1}$) throughout model integration
nosub	$\beta_s = 0$ throughout model integration

Table 2: A list of the three cases examined in this study.

The first part of the study will compare the *nosub* and *sub constant* schemes with the objective of evaluating the effects of a constant β_s parameterization on the model. Physical changes from this parameterization can be measured through state variables and fluxes, whose direction of change is anticipated from Section 2. The study will then examine changes in model performance.

The model performance evaluation consists of two studies. First is an assessment of the model error: a random, time-varying component of all model prognostic ODEs that quantifies missing processes, to be discussed in Section 4. In theory, because subsidence should occupy the set of all missing physical processes contributing to model error in a model without any subsidence parameterization, it is possible that accounting for this process should reduce the model error magnitude. Being a random variable, however, any net change incurred may not necessarily indicate a net improvement because of the unknown nature of the outstanding missing processes. Nonetheless, it is useful to check the model error to evaluate the extent of change

wrought by subsidence inclusion. Such values would also be useful in evaluating mass continuity in the event of advection resolution by the model.

A second test of performance is sensitivity of $\beta_s(t)$ and the final value (β_{sf}) to β_{s_0}. This test will simultaneously examine the convergence of $\beta_s(t)$ solutions and how well the range of β_{s_0} values is reduced during integration by the initial condition estimation procedure (Section 4.b). Reduced RMSE scores of the assimilated variables will provide evidence of improvement across the various sensitivity tests. The RMSE is given by 12:

$$RMSE = \sqrt{\frac{1}{n}\sum_{i=1}^{n}\left(M(y)_i - Z_i\right)^2} \qquad (12),$$

where Z_i is the i^{th} observation of variable Z, n is the total number of assimilated Z observations and $M(y)_i$ is the i^{th} model estimate, mapped to Z. A reduced RMSE score indicates an enhanced capability of the model to match measurement.

The second part of this study is the comparison of the *sub* and *sub constant* cases with the objective of identifying improvement due to the time-varying β_s scheme. The method of experimentation is similar to the first part. However, without observations of subsidence available for comparison, an analysis of the physical changes will not adequately diagnose improvement. Therefore, the second part will focus primarily on model performance to demonstrate success with the time-varying scheme.

As stated in Section 1.c, this experiment seeks to improve the ability to model a non-negligible physical process without the constraints of limited integration time or explicit measurement. Although it is a difficult process to quantify, it does vary slowly in time, thus facilitating the capture of change through parameterization. This study seeks to take advantage of the latter trait and determine if multiple day ABL studies can benefit from this effort toward model physics improvement. This method is expected to provide model improvement versus a case with neglected subsidence (De Ridder 1997, Margulis and Entekhabi 2004) on the basis of enhanced physics. However, the method is also anticipated to provide improvement versus a case with a static β_s parameterization (Stull 1976, Batchvarova and Gryning 1994) because it

attempts to resolve the previously aliased evolution of a physical process. The confirmation of these results will signify the validity of the experiment and justify further studies of a time-varying subsidence parameterization in more complicated, multi-dimensional ABL and coupled models.

4. MODEL

a. *Forward Model*

The one-dimensional coupled land-ABL model of ME01 is chosen to study the effect of time-varying subsidence in the ABL. A complete description of the model is found in ME01 with modifications in Margulis and Entekhabi (2003, hereinafter ME03). The full model consists of a forward model of the coupled land-atmosphere system and its adjoint. Its coupled nature allows for the solution of energy and moisture budget equations at the land surface and in the ABL, which become the model prognostic ODEs. The set of all forward model prognostic equations can be described as:

$$\frac{d\mathbf{y}}{dt} = \mathbf{F}(\mathbf{y}) + \boldsymbol{\omega}(t) \qquad (13),$$

where $\mathbf{y}(t)$ is the state vector, $\mathbf{F}(\mathbf{y})$ is a nonlinear vector that is a function of all model states and $\boldsymbol{\omega}(t)$ is the time-varying, unknown model error attributed to $\mathbf{y}(t)$. The initial (prior) model error is set to zero. Figure 1 depicts a schematic of the model mechanics.

The atmospheric component of the governing equations is captured by (4) through (10), introduced in Section 2. It consists of a slab mixed layer atop the land surface (no surface layer included). The ABL energy budget is represented by a prognostic equation for potential temperature (θ) and the ABL moisture budget is represented by a prognostic equation for specific humidity (q). In addition to ground (H_g, E_g), canopy (H_c, E_c) and entrainment fluxes (H_{top}, E_{top}) handled by both prognostic equations, the

energy budget includes a thorough treatment of incoming shortwave and outgoing longwave radiative fluxes.

The ABL energy and moisture budget equations are complemented by a prognostic equation for mixed layer height (h). The mixed layer height is coupled to the free atmosphere through two final prognostic equations governing the 'jump' in potential temperature (δ_θ) and specific humidity (δ_q) at the top of the ABL. These 'jumps' are requisite features in a slab ABL model that describe the relative strength of the inversion across the ABL-free atmosphere boundary.

Unique to this study is the addition of an eighth ABL prognostic equation, that of the subsidence parameter, defined by (14):

$$\frac{d\beta_s}{dt} = \omega_{\beta_s} \tag{14}.$$

The model error component of the forward model prognostic equation is a single term substitute for the conglomerate of missing physics presumed to mar the formula. The calculation of this term and the origin of (14) are found in the adjoint model, detailed in Section 4.b. Although non-zero model error exists in all prognostic equations (4-10 and 14), in this study it is solved only for the θ, q and β_s (4, 5 and 14 respectively). This is because a lack of advection is presumed to dominate the missing model physics terms (Margulis and Entekhabi 2004). Thus, the variables/parameters most sensitive to advection (θ, q) and mass continuity (β_s) possess a model error component in their ODE.

The land surface prognostic equations, which remain unchanged from the ME01 settings, can be found in Appendix B. The land surface component consists of three energy prognostic equations and three moisture budget equations. The three energy prognostic equations solve for canopy temperature (T_c), ground temperature (T_g) and deep soil temperature (T_d) while implicitly treating effects of vegetation. The three moisture budget equations solve for soil moisture at three discrete levels (W_1, W_2, W_3), all within two meters of the surface.

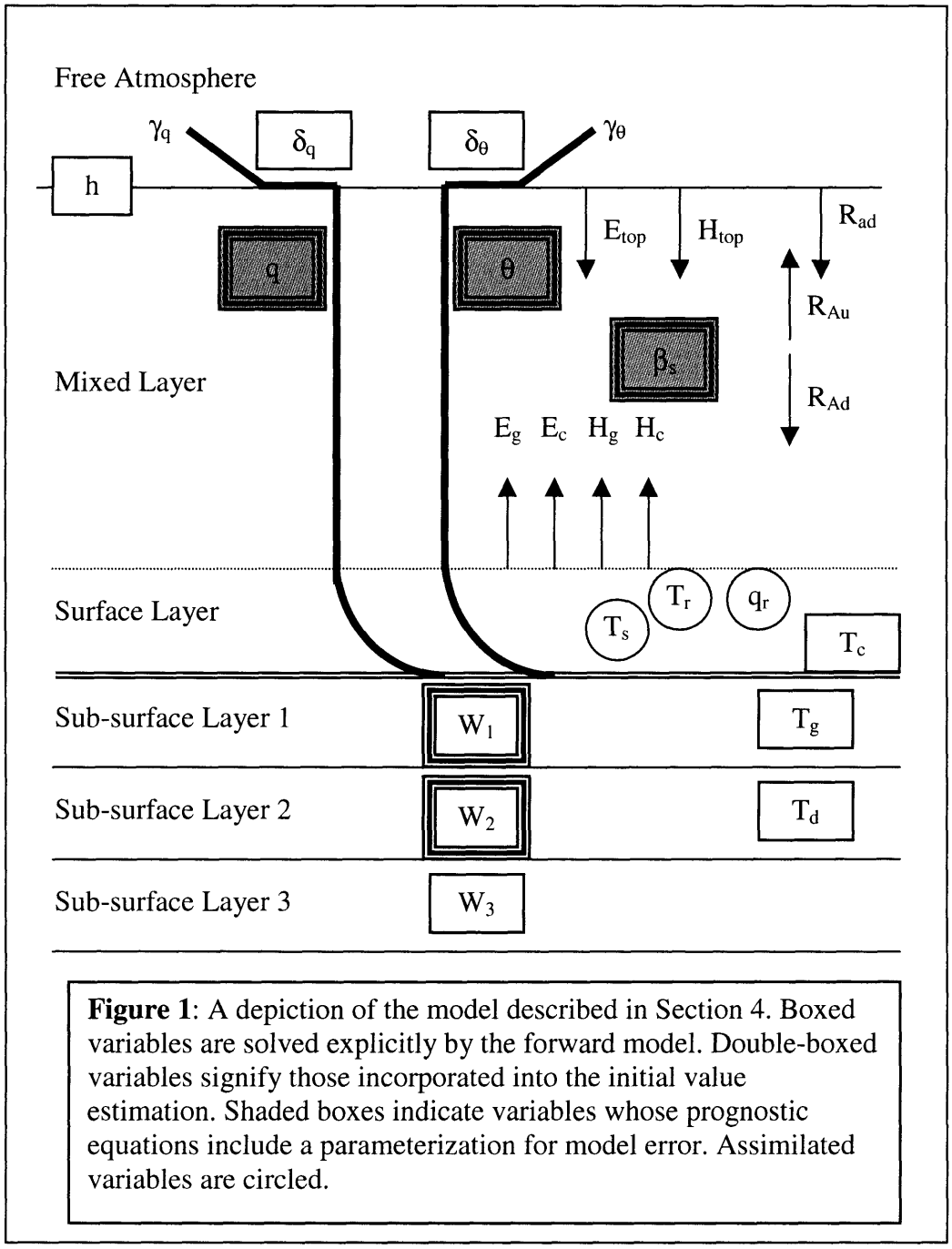

Figure 1: A depiction of the model described in Section 4. Boxed variables are solved explicitly by the forward model. Double-boxed variables signify those incorporated into the initial value estimation. Shaded boxes indicate variables whose prognostic equations include a parameterization for model error. Assimilated variables are circled.

The model requires a minimal high sampling frequency supporting dataset to force the prognostic equations. Specifically, the model requires top-of-the-ABL solar irradiance, large-scale wind speed, accumulated precipitation and surface pressure. These time-variant terms are inserted into the forward model at each time step.

b. *Adjoint Model*

From the forward model prognostic equations, the model state variables will evolve a temporal solution of the 1-D coupled land-ABL system. However, regardless of the precision of initial conditions, this is no certainty that this system will accurately reflect a true dynamical evolution. By assimilating time-varying data into the model, it is possible to adjust the model solution toward the measurements for the purpose of bringing the model solution (mapped to the measurements) closer to truth. Data assimilation, and the process of minimizing the model-measurement misfit requires the development of a parallel model.

Building off the state vector prognostic (13), the initial condition vector also accounts for unknown processes corrupting the estimate. The initial condition vector for model state variables is defined as:

$$\mathbf{y}(t_0) = f(\boldsymbol{\beta}) \qquad (15),$$

where $\boldsymbol{\beta}$ is a time-invariant random (unknown) vector. As in traditional data assimilation methods such as the Kalman filter, The two unknown vectors, $\boldsymbol{\omega}(t)$ and $\boldsymbol{\beta}$, are initially classified by their mean values $(\bar{\boldsymbol{\beta}})$ and $(\bar{\boldsymbol{\omega}}(t))$ and their covariances ($\mathbf{C}_{\beta}$ and $\mathbf{C}_{\omega}((t,t'))$. The structure of each covariance is detailed in Appendix C. The mean values represent the best estimates of prior knowledge of the parameters and the covariances represent the best estimates of prior uncertainty.

The relationship of the observations and model states is given by:

$$\mathbf{Z} = \mathbf{M}(\mathbf{y}) + \boldsymbol{\nu} \qquad (16),$$

where $\boldsymbol{Z}$ is the measurement vector, $M(y)$ is the measurement operator that maps model states onto measurements and ν is the time-invariant, unbiased measurement

error attributed to $\boldsymbol{Z}$. ME03 thoroughly describe the production of $\boldsymbol{M(y)}$ for the observations assimilated in this study. In this study, as in ME03, the measurement vector, $\boldsymbol{Z}$, consists of radiometric surface temperature observations and 2 m temperature and specific humidity observations, detailed in Section 4.c. The measurement errors are assumed to be unbiased and are given by a covariance $\boldsymbol{C_v}$.

To minimize the misfit between a measurement and model estimate, one can invoke calculus of variations. The general problem can be classified by (17), often described as a model response functional:

$$J = \int_t f(\mathbf{y}, \boldsymbol{\alpha}) dt \quad (17). \qquad (17),$$

where J is a non-dimensional scalar and f is a nonlinear function of the N_s state variables ($\boldsymbol{y}$) and model parameters ($\boldsymbol{\alpha}$).[4] The minimization of (17) is not an independent process, however. It must obey the state vector function (13) lest it violate the physics of the problem. Thus, (13) acts as a constraint on (17). Hence, there exists a constrained optimization problem with N_s independent variables and N_s constraints.

Given a large set of independent variables, the most expedient way to determine the global minimum of a constrained optimization problem is the method of Lagrange. This method consists of introducing a Lagrangian function (L) that juxtaposes the function to be minimized ($g(\boldsymbol{y})$) with its constraint/s. We define the Lagrangian function:

$$L = g(y_1, y_2, y_3, \ldots y_{N_s}) + \lambda \phi(x_1, x_2, x_3, \ldots x_{M_s}) \qquad (18),$$

where λ is the Lagrange multiplier, a constant that is unique to the constraint $\phi(x_1, x_2, x_3, \ldots x_{Ms})$, which is a function of M_s independent variables that may or may not be coincident with variables $\boldsymbol{y}$ of $g(\boldsymbol{y})$. Note that $g(\boldsymbol{y})$ can exist subject to any number of constraints (ϕ), where each new constraint requires a unique Lagrange multiplier (λ); such additional constraint terms are additively appended to (18).

[4] Note that this objective function J need not only apply to model-measurement discrepancies but may also be used to create convergence of unknown parameters or vectors.

In the coupled land-ABL model, there are 12 state variables/parameters solved and thus there must be 12 unique Lagrange multipliers, each one corresponding to the constraint function (12) as applied to each of the 12 state variables. The model response functional is adjoined to the constraint as:

$$L = \int_t f(\mathbf{y},\alpha)\,dt + \int_t \lambda\left[\frac{d\mathbf{y}}{dt} - F(\mathbf{y}) - \boldsymbol{\omega}\right]dt \qquad (19).$$

The Lagrange multipliers, by virtue of their role in the adjoining of the model response functional and the constraining function in the Lagrangian function are labeled as adjoint variables. In this study, the model response functional (17) consists of the model components to be minimized. Substituting these components into the Lagrangian (19) results in (20):

$$\begin{aligned} J' = {} & [\mathbf{Z} - \mathbf{M(y)}]^{\mathrm{T}}\mathbf{C}_v^{-1}[\mathbf{Z} - \mathbf{M(y)}] + \left(\boldsymbol{\beta} - \bar{\boldsymbol{\beta}}\right)^T \mathbf{C}_\beta^{-1}\left(\boldsymbol{\beta} - \bar{\boldsymbol{\beta}}\right) + \\ & \int_0^f \int_0^f \boldsymbol{\omega}(t')^T \mathbf{C}_\omega^{-1}(t',t'')\boldsymbol{\omega}(t'')dt'dt'' + 2\int_0^f \lambda^T\left[\frac{d\mathbf{y}}{dt} - \mathbf{F(y)} - \boldsymbol{\omega}\right]dt \end{aligned} \qquad (20),$$

where the (J') follows conventional nomenclature for this expression, also known as an objective function or performance index. The first expression represents the misfit between measurements ($\mathbf{Z}$) and model estimates ($\mathbf{M(y)}$). The second term impairs minimization when the initial condition random vector deviates from prior values. The third term provides a similar effect but for the time-varying random model error. The final term carries over from the earlier Lagrangian expression in (19). The assimilation window [t_0, t_f] corresponds to the forward model integration limits.

The adjoint model, designed to solve for the adjoint variables required to define and minimize the objective function, evolves from the first variation of (18) and is given by (21):

$$\frac{\partial \boldsymbol{\lambda}}{\partial t} = -\left(\frac{\partial \mathbf{F}}{d\mathbf{y}}\right)^T \boldsymbol{\lambda} - \left(\frac{\partial \mathbf{M}}{\partial \mathbf{y}}\right)^T [\delta]\mathbf{C}_v^{-1}[\mathbf{Z} - \mathbf{M(y)}] \qquad (21),$$

where [δ] is the diagonal matrix of Dirac delta functions. The starting value of the backwards integrating adjoint model ($\lambda_f \equiv \lambda(t_f)$) is set to zero because the model

response cannot be measured beyond the limits of integration. However, it also unfairly biases the adjoint variable boundary conditions to zero, which causes bias in the model error curves, discussed later.

From the adjoint variable solutions provided by (21), one can calculate the gradient of the objective function with respect to the unknown vectors $\omega(t)$ and β given by (22) and (23):

$$\frac{\partial J}{\partial \boldsymbol{\beta}} = \left(\boldsymbol{\beta} - \bar{\boldsymbol{\beta}}\right)^T \mathbf{C}_\beta^{-1} - \left(\frac{\partial \mathbf{f}}{\partial \boldsymbol{\beta}}\right)^T \boldsymbol{\lambda}_0 \qquad (22),$$

$$\frac{\partial J}{\partial \boldsymbol{\omega}(t)} = \int_0^{t_f} \boldsymbol{\omega}(t')\mathbf{C}_\omega^{-1}(t',t)dt' - \boldsymbol{\lambda}(t) \qquad (23),$$

where C_β is the initial condition error covariance and C_ω is the model error covariance. These gradients, in turn, are used to minimize the objective function and hence reduce model-measurement misfit. The minimization results from the convergence of $\omega(t)$ and β through an iterative gradient search algorithm. Using a steepest descent method given by (24):

$$u_p^{k+1} = u_p^{k} - \varepsilon\left(\frac{\partial J}{\partial u_p}\right)^k \qquad (24),$$

where u_p is any parameter and ε is the (arbitrary) scalar step size, ME03 solves the update (25) and (26) corresponding to (22) and (23), respectively:

$$\boldsymbol{\beta}^{k+1} = \boldsymbol{\beta}^k - \eta_\beta\left(\boldsymbol{\beta}^k - \bar{\boldsymbol{\beta}}\right) + \eta_\beta \mathbf{C}_\beta \left(\frac{\partial \mathbf{f}}{\partial \boldsymbol{\beta}}\right)^T \boldsymbol{\lambda}_0^k \qquad (25)$$

$$\boldsymbol{\omega}^{k+1}(t) = \left(1 - \eta_\omega\right)\boldsymbol{\omega}_k(t) + \eta_\omega \int_0^{t_f} \mathbf{C}_\omega(t,t')\boldsymbol{\lambda}^k(t')dt' \qquad (26),$$

where k is the iteration step and $\eta_i = \varepsilon_i / C_i$ (where C_i is the variable's uncertainty covariance). The iteration process itself involves four steps: (1) integrate the forward model with prior values, (2) integrate the adjoint model backwards in time using

updated states, (3) compute the performance index gradients to update β and $\omega(t)$ and (4) repeat steps (1)-(3) until reasonable numerical convergence is reached for β corresponding to the initial condition of the state variables with the longest memory: (θ, q, W_1, W_2 and β_s). As described in Section 4.a, model error is solved only for those variables presumed to have a significant influence on missing physical processes (e.g., θ, q, and β_s).

As described in (14), model error ($\omega_{\beta s}$) drives the evolution of β_s. In the solution of $\lambda_{\beta s}$ (21), the only non-zero component is $\frac{dh}{d\beta_s}\lambda_h$. This expression determines the evolution of $\lambda_{\beta s}$, which, by (26), defines $\omega_{\beta s}$. Thus, the time-evolution of β_s is shifted according to the model response to the parameter, expressed through the adjoint variable $\lambda_{\beta s}$. In effect, the parameter responds to model guidance in determining its temporal evolution, starting from β_{s_0}. Recall that β_{s_0} is calculated through the initial condition estimation process, designed to converge on the optimal solution for β_{s_0} and four other variables described above.

c. *Dataset*

The model estimates are optimized through a suite of observations suitable for data assimilation. The First International Satellite Land Surface Climatology Project (ISLSCP) Field Experiment (**FIFE**) study done in Kansas, USA in the summers of 1987 and 1988 (Sellers et al. 1992) includes a dataset capable of providing all the necessary observations to be assimilated in this study (Betts and Ball 1998). Specifically, FIFE data provides surface radiometric temperature (T_s), and reference level (2 m) temperature (T_r) and specific humidity (q_r) observations, all at 30-minute intervals. Two three-day periods of continuous, valid observations were readily available: 4-6 June and 15-17 August 1987. These periods were chosen in part because they represent dry periods to avoid potential complications due to cloud cover (Betts 2000). However, these periods were used principally for early calibration studies.

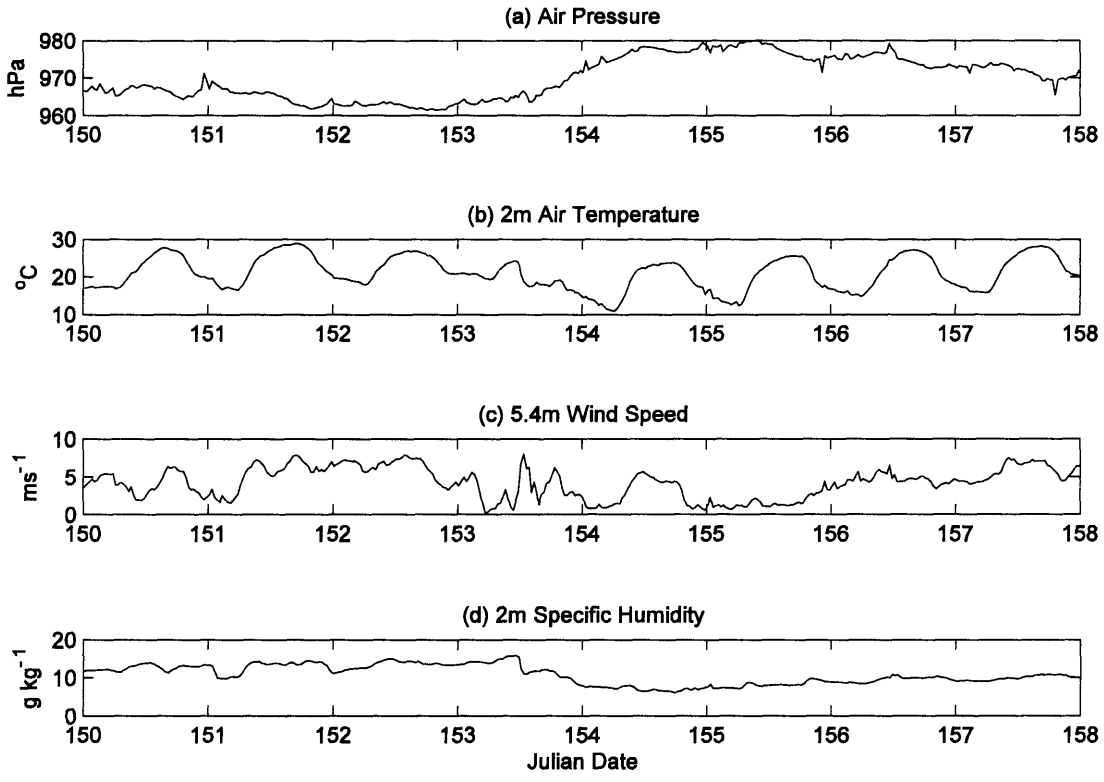

Figure 2: Plots of key weather observations at the FIFE site for the period of study in 1987. Dates given are in local time (CDT).

The eight day period of 30 May – 6 June 1987 (day of year 150-157) provides the longest, driest window of one week or greater during the season of observation. The longer period is also equivalent to two synoptic time scales, which is ideal for this study as discussed in the Sections 1 and 3.

FIFE also provides the radiosondes observations of W. Brutsaert (Strebel et al. 1994), launched at approximately 90-minute intervals during intensive field campaigns. The period 30 May – 6 June 1987 contains a fair continuity of available radiosondes data. By fitting an average of the early morning soundings in the ABL to a quadratic function of h, the free atmosphere lapse rates needed in the forward model (γ_θ and γ_q) have unique solutions each day that vary according to h. These estimates do not evolve during the day, however, leaving open the possibility of error due to advection or other local changes.

Figure 2 provides a sample of local meteorological data for the period 30 May – 6 June 1987. Taken from FIFE (Betts and Ball 1998) Subplots (a) through (d) show a time series of surface air pressure, 2 m temperature, 5.4 m wind speed, and 2 m specific humidity.

5. RESULTS

a. *Effects of a constant β_s parameterization*

Figure 3 presents results designed to verify the net effects of subsidence anticipated from theory. The subplots (a) through (e) depict the eight-day time series of θ, q, δ_θ, δ_q and h as they differ between a model integration with a constant β_s value (*sub constant*) and without any subsidence parameterization (*nosub*). The figure indicates a clear net warming and reduction of mixed layer depth. In addition, as anticipated from theory, the inversion strength at the top of the boundary layer weakens for both δ_θ and δ_q. There is also a slight net moistening of the ABL, to be discussed in Section 6.

Figure 4 also presents an example of the net effect of subsidence through an examination of the energy budget (a) and moisture budget (b) as defined through the flux components of (4) and (5), respectively. Results from this figure indicate a net reduction of surface sensible heat flux together with a slight reduction of the sensible heat entrainment to balance out the net warming induced by a reduced mixed layer depth. In the moisture budget, an enhanced dry air entrainment is present as the result of including a subsidence parameterization, supporting a net drying along with the reduced mixed layer depth. However, the net increase in surface latent heat flux serves to counter this effect slightly.

Table 3 offers a more quantitative summary of the physical changes incurred by the model resultant from a constant β_s subsidence parameterization. These values serve to complement Figure 3 and 4 by displaying the mean change incurred by a series of selected state variables and fluxes. The change is separated by the diurnal time scale due to the diminished effect of the subsidence parameterization in the nocturnal boundary layer.

In addition to the more obvious physical changes wrought by the implementation of a subsidence parameterization, it is also necessary to evaluate changes to model performance, including the model error and the assimilated variables' RMSE. Figure 5a (b) presents the model error from the $\theta(q)$ prognostic equation for the *sub constant* and *nosub* cases. A clear disparity exists across most of the period for both the θ and q curves, with the *sub constant* case mostly demonstrating improvement. Finally, Figures 6a, 6b and 6c offer a comparison of the *sub constant* and *nosub* cases via RMSE for T_r, q_r and T_s, respectively. As with the inspection of model physics in Figure 5, Figure 6 further justifies model improvement with an apparent of reduction of RMSE for T_r and q_r, the variables most influenced by large-scale ABL divergence

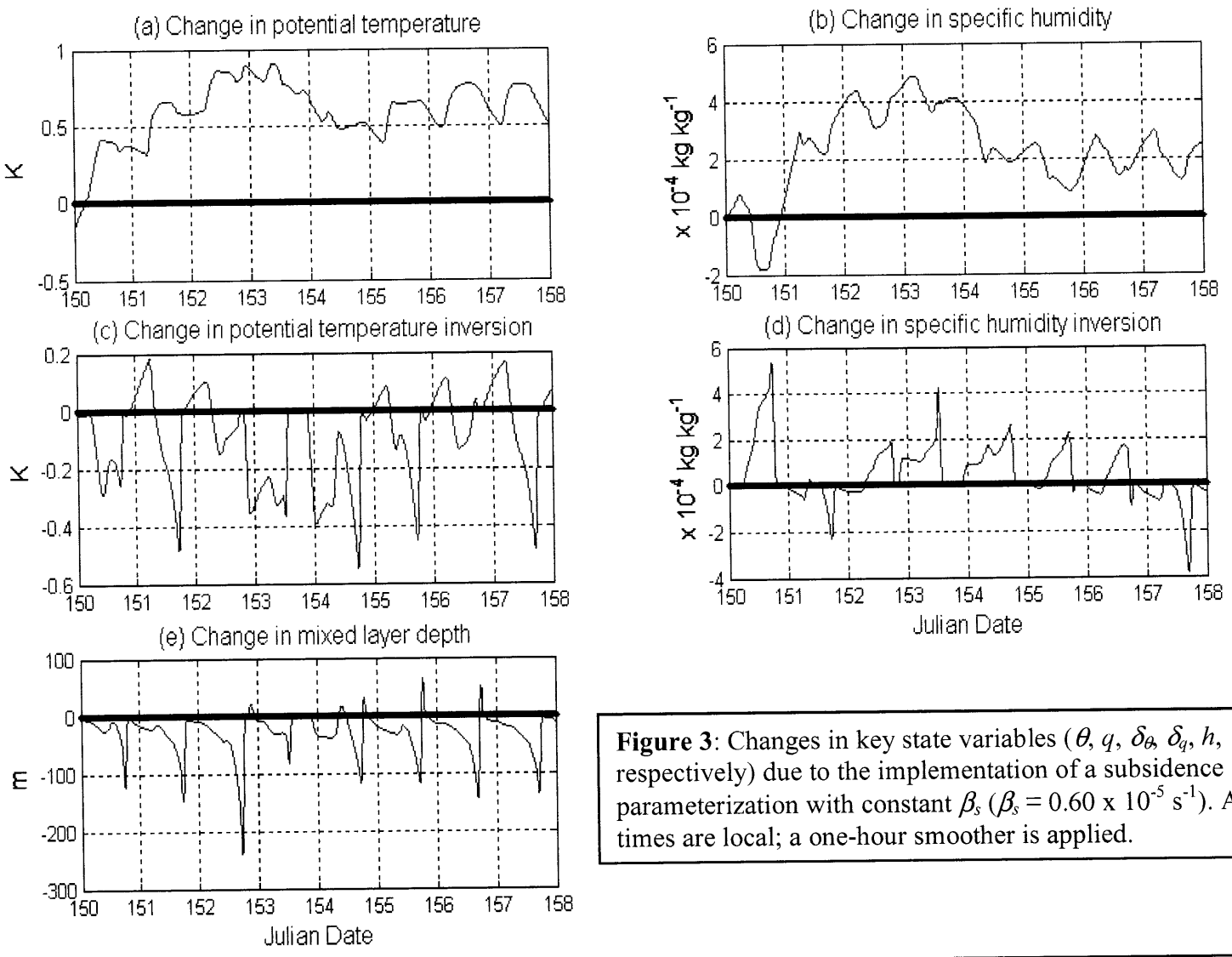

Figure 3: Changes in key state variables (θ, q, δ_θ, δ_q, h, respectively) due to the implementation of a subsidence parameterization with constant β_s ($\beta_s = 0.60 \times 10^{-5}$ s^{-1}). All times are local; a one-hour smoother is applied.

b. Effects of a time-varying β_s parameterization

The parameterization of subsidence is expected to provide non-negligible model improvement by virtue of the improved (i.e., no longer neglected) physics. These changes in physics were verified in Section 5.a. It is also anticipated that a time-varying β_s estimation process should outperform a constant β_s scheme because the former will account for changes in the evolution of large-scale subsidence over time. One key indicator of the physical change from a time-varying β_s approach is the subsidence velocity. Figure 7 depicts the model estimated mean ABL subsidence velocity, calculated from (11) at each timestep (Δt = 1 min.) in the forward model. The magnitude of the subsidence parameter used to create these charts is taken from the midpoint of the range of initial draws that produces the best convergence of $\beta_s(t)$ in time under the time-varying scheme, to be discussed in Section 5.b (also see Figure 9). The value is $\beta_{s_0} = 0.60 \times 10^{-5} s^{-1}$.

Without a thorough observational record of subsidence against which to compare these results, it is difficult to assess the superiority of the time-varying scheme from change to state variables alone. To determine whether a time-varying β_s results in improvement to the model, it is necessary to evaluate model performance. Figure 8 depicts the time-series evolution of the model error. Subplot (a) depicts the time-varying β_s (*sub*) and *sub constant* cases of model error for θ, (b) shows the same for q and (c) shows the model error for β_s. Unlike Figure 5, Figure 8 does not depict a clear reduction in the magnitude of model error. The model error increases in the case of ω_q, and incurs negligible change in the case of ω_θ. Further discussion follows in Section 6.

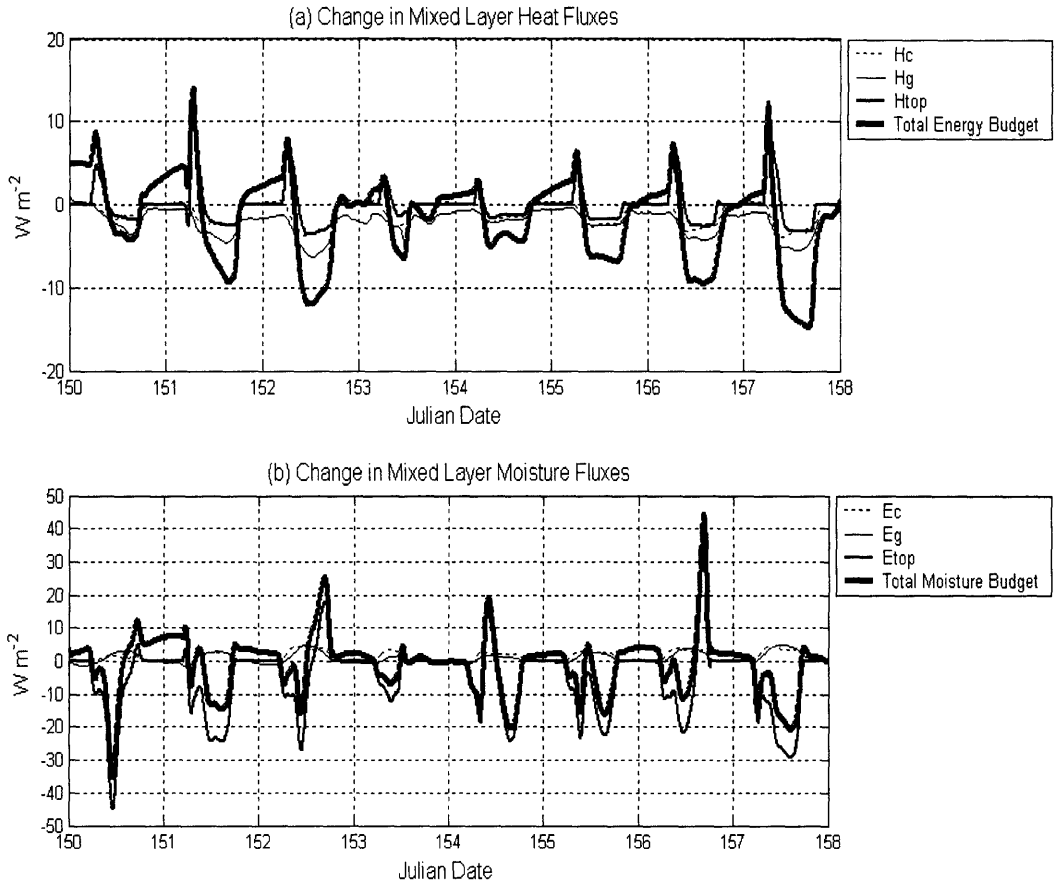

Figure 4: Changes in ABL fluxes due to the implementation of a subsidence parameterization with constant β_s ($\beta_s = 0.60 \times 10^{-5}$ s^{-1}). All times are local; a one-hour smoother is applied. Subplot (a) shows change in canopy (H_c) and ground (H_g) sensible heat fluxes, sensible heat entrainment (H_{top}) and the total ABL energy budget. Subplot (b) shows change in canopy (E_c) and ground (E_g) latent heat fluxes, dry air entrainment (E_{top}) and the total ABL moisture budget.

Quantity	Symbol	Units	Effect of Subsidence			
			Daytime		Nighttime	
			Mean	Standard Deviation	Mean	Standard Deviation
Mixed layer potential temperature	θ	[K]	0.65	0.16	0.52	0.22
Sensible heat entrainment	H_{top}	[Wm^{-2}]	-0.21	2.85		
Canopy sensible heat flux	H_c	[Wm^{-2}]	-1.75	1.14	0.23	0.17
Ground sensible heat flux	H_g	[Wm^{-2}]	-2.78	1.45	-0.92	0.59
Potential temperature inversion	δ_θ	[K]	-0.15	0.14	-0.02	0.15
Mixed layer specific humidity	q	[10^{-4} kg kg^{-1}]	2.15	1.50	2.50	1.35
Dry air entrainment	E_{top}	[Wm^{-2}]	-9.10	11.78		
Canopy latent heat flux	E_c	[Wm^{-2}]	2.25	1.25	0.10	0.20
Ground latent heat flux	E_g	[Wm^{-2}]	1.73	1.54	-0.21	0.51
Specific humidity inversion	δ_q	[10^{-4} kg kg^{-1}]	0.81	1.36	0.05	0.51
Mixed layer depth	h	[m]	-38.34	40.44	-14.46	9.56

Table 3: The net effect of subsidence parameterization with constant β_s ($\beta_s = 0.60 \times 10^{-5}$ s^{-1}) on selected components of the coupled model. Mean change is calculated separately for daytime (between the time when entrainment begins and the time when the late afternoon ABL collapse transition period ends) and nighttime (the complementary period). The mean is calculated over a continuous eight-day period (Julian Day 150-157, see Section 4.c). Each mean value is accompanied by a standard deviation. Note that a net increase of δ_q corresponds to a weakened inversion (less negative).

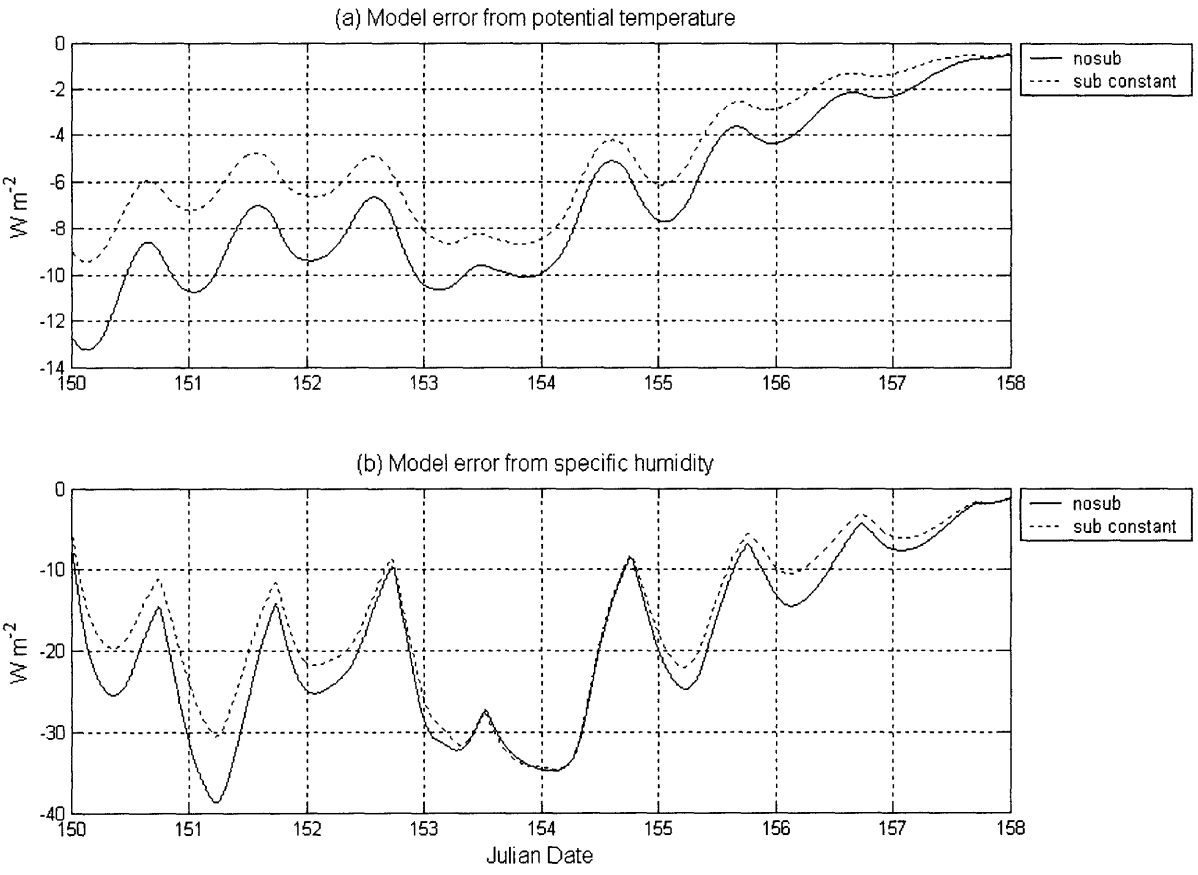

Figure 5: Model error (ω) from the potential temperature prognostic equation (a) and the specific humidity prognostic equation (b) compared between a subsidence parameterization with constant β_s (*sub constant*) and no parameterization for subsidence (*nosub*)

To better understand the robustness of this model enhancement, it is necessary to evaluate its sensitivity. One key check for convergence of solution is a test of sensitivity to initial conditions. Figure 9 shows the evolution of $\beta_s(t)$ using a systematic sample of draws from a range of β_{s_0} believed to best represent the ambient atmospheric conditions. This test is completed for the both the *sub* and *sub constant* cases. RMSE scores for all assimilated variables (T_r, q_r, T_s) help to gage the effect of various β_{s_0} on model performance. The degree to which the curves converge in time from the array of initial value estimates is fairly slow. As will be discussed in Section 6, this may be due both to the model error covariance decorrelation time scale in conjunction with the length of the model integration. Figure 10 depicts the RMSE score as a function of the tested β_{s_0} values for (a) T_r, (b) q_r and (c) T_s for the *sub* and *sub constant* cases. The improvement here over the *sub constant* case is mixed. Only q_r demonstrates an consistency of RMSE reduction, but even then the improvement is only slight.

6. ANALYSIS

a. *Constant β_s versus no subsidence parameterization*

Figure 3a confirms a clear net warming due to subsidence throughout the period, as anticipated from theory. The warming averages about +0.65°C during the daytime (see also Table 3). Less expected is the result in Figure 3b, showing changes to the mixed layer q. Although a diurnal minimum is consistently present in the late afternoon, the net change is almost entirely positive (net moistening). This net change is small, however, averaging about two orders of magnitude less than the ambient conditions (Figure 2d). Examining the inversion terms in Figures 3c and 3d, there is a conspicuous daytime reduction of δ_θ, but only a slight daytime increase of δ_q, thus decreasing the magnitude of the inversion in both cases, with obvious implications for entrainment, as will be seen later. As expected, the mixed layer height is reduced substantially by subsidence, seen in Figure 3e. Reductions of nearly 100m are common in the late afternoons just before ABL collapse. Note that in Figures 3c, 3d

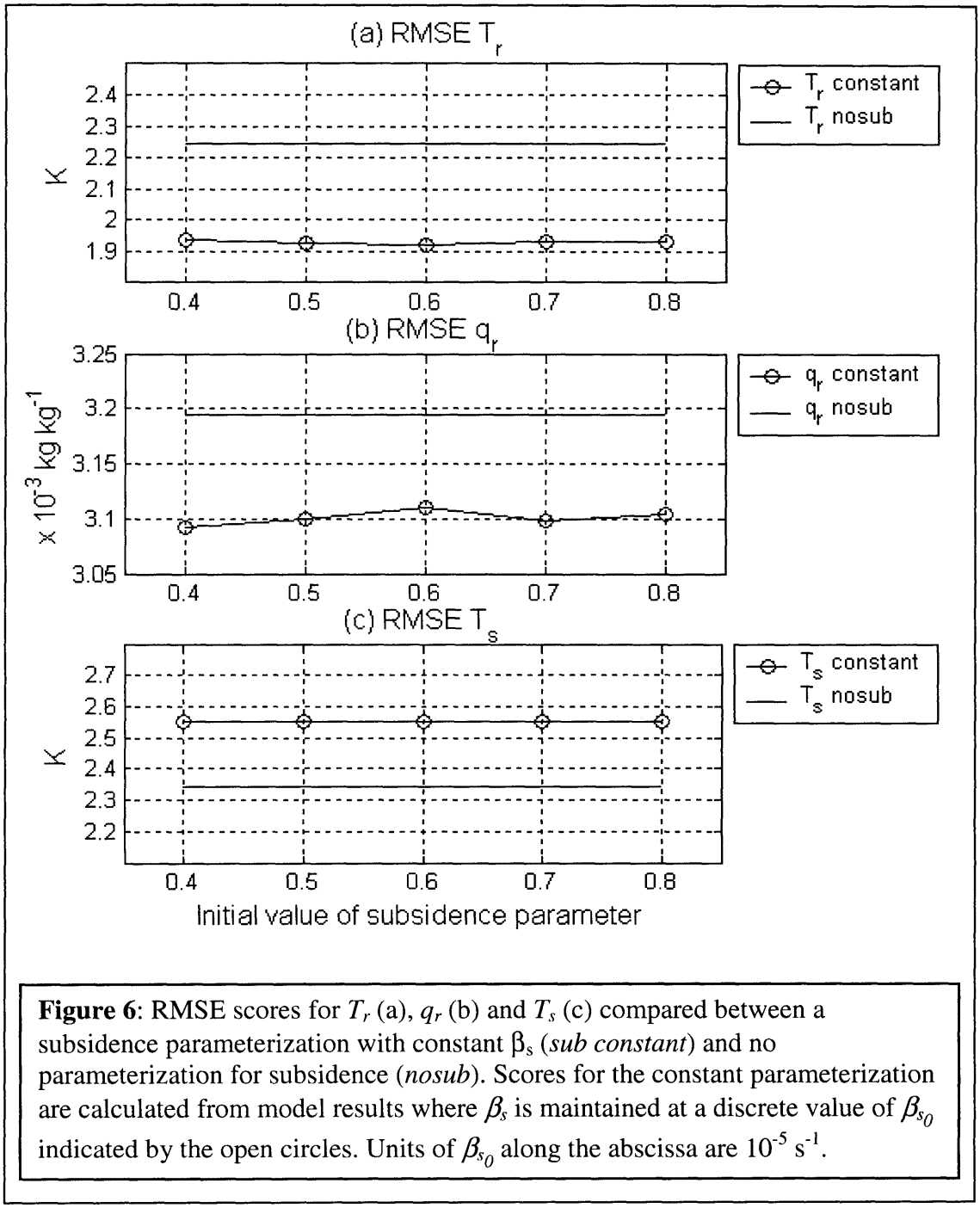

Figure 6: RMSE scores for T_r (a), q_r (b) and T_s (c) compared between a subsidence parameterization with constant β_s (*sub constant*) and no parameterization for subsidence (*nosub*). Scores for the constant parameterization are calculated from model results where β_s is maintained at a discrete value of β_{s_0} indicated by the open circles. Units of β_{s_0} along the abscissa are 10^{-5} s^{-1}.

and 3e there is a conspicuous discontinuity near the time of ABL collapse each day. This jump results from a slight change to the time of collapse owing to subsidence inclusion and, thus, the significant discontinuity in the state variables. In general, these results are typical of what was expected from theory. One can examine these changes in more detail by studying the net changes to the ABL energy and moisture budgets.

Figure 4a depicts the net change to the heat flux terms that define (4). The ground flux changes are consistently negative, but with a strong tendency toward nocturnal neutrality. This is likely because of the net ABL warming that reduces the surface temperature gradient most during the daytime. The canopy fluxes follow suit, though smaller in magnitude and very near zero at night. This follows theoretical expectations exactly. It is clear, however, that the variable most responsible for the behavior of the total energy budget (the left-hand-side term of (4)) is the net change to sensible heat flux entrainment. At dawn, at the start of mixed layer growth, the previously negated term presents a substantial net positive forcing on the budget, quickly decaying into a net negative forcing, as expected from the effect on θ inversion in Figure 3c. From theory, and based on the net warming observed in Figure 3a, it is likely that the diurnal-averaged net change to H_{top} does little to reduce temperature in the ABL compared to the effects of h reduction, hence the warming in Figure 3a.

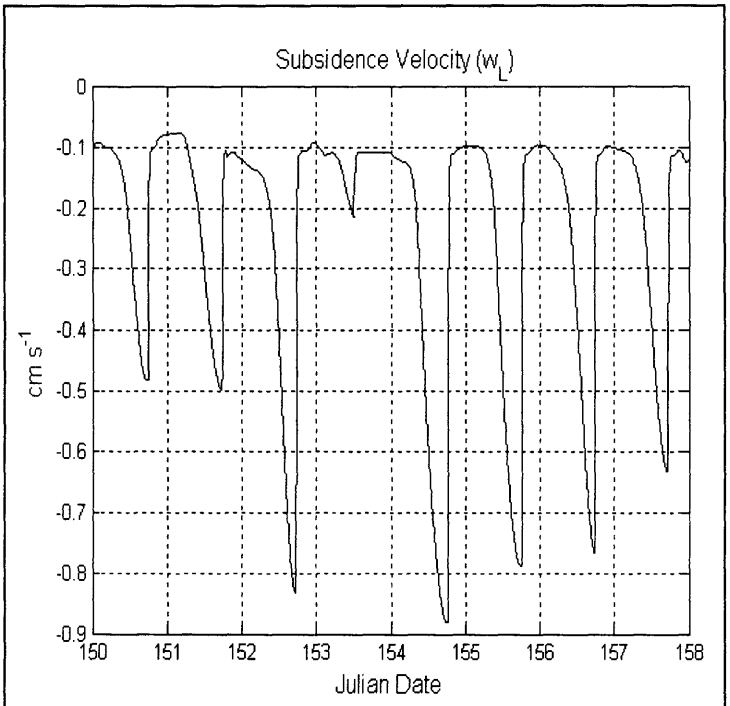

Figure 7: Subsidence velocity estimated from a time-varying subsidence parameterization (β_{s_0} = 0.60 x 10^{-5} s^{-1}). All times are local.

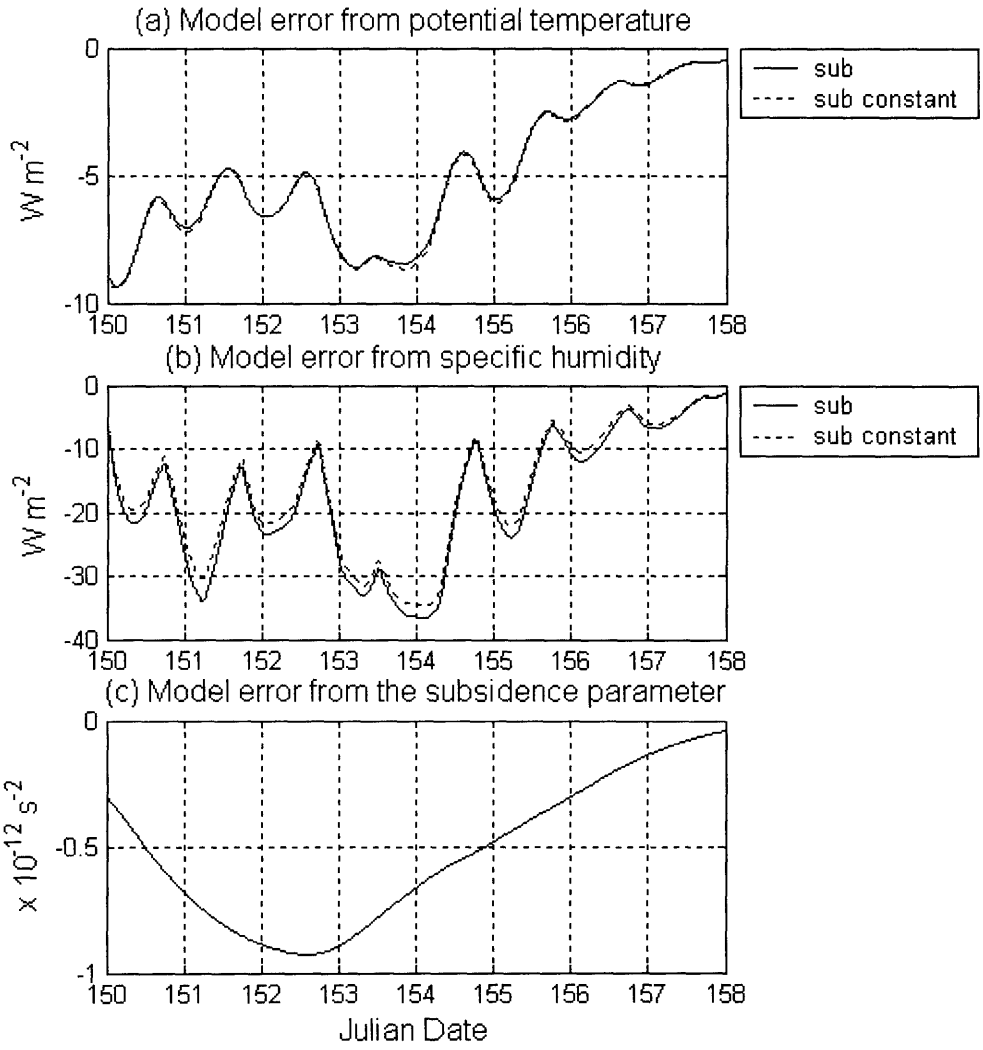

Figure 8: Model error (ω) from the potential temperature prognostic equation (a), the specific humidity prognostic equation (b) and the subsidence parameter prognostic equation (c) compared between a subsidence parameterization with a time-varying β_s (*sub*) and a constant β_s parameterization (*sub constant*).

Figure 4b confirms the expected net negative effect of subsidence on E_{top} (enhancing latent heat entrainment), in general. There is also a very consistent daytime net increase from the surface latent heat fluxes, as anticipated from theory. Figure 4b also depicts a good deal of E_{top} fluctuation during the daytime, however. Specifically, on Days 152 and 156, there is a late afternoon spike in E_{top} for reasons that are unclear, though likely attributed to the substantial collapse-time h discrepancies. Looking at the total moisture budget term (e.g., the left-hand-side of (5)), it is apparent that these fluxes serve to increase the net moisture in the ABL column, confirmed by the net change to q in Figure 3b.

The physical effects of subsidence anticipated from theory are evident in the model output. Table 3 confirms an average net ABL warming through the period of more than 0.50 K from the significant mixed layer depth reduction. The warming is tempered by the reduction in surface sensible heat fluxes from the ground and canopy as well as the reduced sensible heat entrainment. In the moisture budget, the theoretical net change due to subsidence was somewhat nebulous. Model estimates indicate a slight net moistening of the ABL. This may be due, in part, to the net increase of surface moisture fluxes from the ground and canopy. Note that the net changes to the surface and entrainment fluxes diminish greatly at night, when change to the mixed layer depth is minimal. Mixed layer depth reductions are significant, averaging over 38 m through the daytime ABL, clearly driving the changes observed in the energy and moisture budgets displayed in Table 3.

The key to verifying a net improvement to model physics is to examine the model performance in the presence of the new subsidence parameterization. This is achieved principally through an evaluation of RMSE scores for the assimilated variables, where the best performance will coincide with the smallest scores as based on the objective of the performance index described in Section 4.b. Though not always coincident with the best model performance, a critical unknown parameter subject to change in the presence of improved physics is the random, time-varying model error vector: $\boldsymbol{\omega}(t)$. Figure 5a shows that subsidence provides a notable improvement of ω_θ. There is a continuous reduction of $|\omega_\theta|$ by an average of 1.8 Wm^{-2}, over 3.0 Wm^{-2} in

places. There is also a consistent reduction of ω_q, seen in Figure 5b, by an average of 2.4 Wm^{-2}, more than 8.0 Wm^{-2} in places. One theme resonant across both Figures 5a and 5b is that $|\omega|_{sub\_constant} < |\omega|_{nosub}$, thus indicating a net reduction of model error with no significant change to the behavior of the curve.

Figure 6 confirms a general net model improvement from a constant β_s parameterization via RMSE scores. Using a range of β_{s_0} estimates comparing across the *sub* and *sub constant* schemes, there is a consistently formidable RMSE score reduction for the two assimilated measurements most closely affiliated with mean ABL divergence: T_r (Figure 6a) and q_r (Figure 6b). The surface temperature measurement, T_s, incurs a net gain of RMSE (Figure 6c). However, skin temperature model estimates are generally governed by surface parameterizations, moisture and radiative fluxes. Thus, it is not unexpected that an improvement to the large-scale

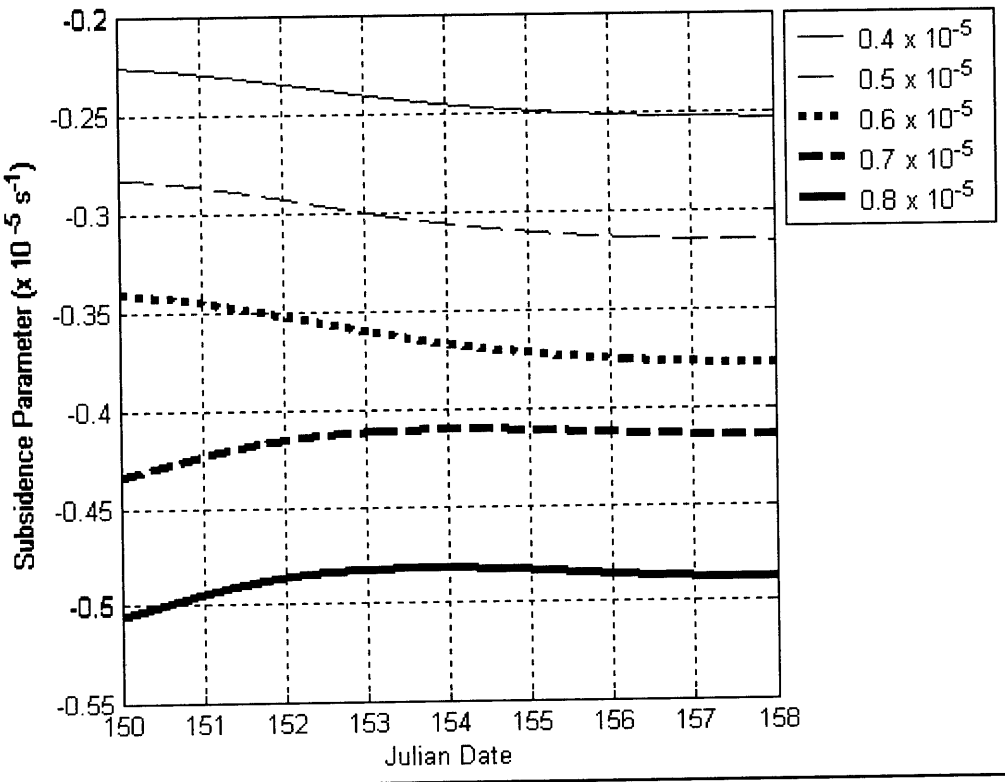

Figure 9: A comparison of subsidence parameter evolutions from a systematic draw of initial values designed to reflect initial uncertainty in a time-varying subsidence parameterization. The curves are defined in the legend by their initial value. Note that because β_{s0} is refined by the initial value estimation scheme, the final iteration's initial value will likely differ from that value assigned prior to the first iteration.

ABL dynamics does not translate to a similar improvement at the surface. Figures 5 and 6 clearly demonstrate the potential influence of a subsidence parameterization on improving model physics and model performance, hence justifying the investigation of a time-varying β_s parameterization.

From these results, it is clear that ABL subsidence plays a non-trivial role in the dynamics of the model set to the conditions at FIFE. The consistent net warming and substantial net h reduction warrant adequate subsidence parameterization. The decisive model improvement shown by the implementation of a constant β_s parameterization further supports additional investigation. The next step is to examine whether a time-varying β_s solution will help improve the ability to model these net changes.

b. Comparing time-varying β_s and constant β_s

The improvement of model physics and model performance from the inclusion of a constant large-scale ABL divergence parameterization to solve the mean ABL subsidence present in the period of study (a.k.a., subsidence parameterization) was expected and is evident in the model estimates. The more tenuous postulate is that a time-varying subsidence parameterization (whereby both β_s and h vary in time) will further improve upon the results of a constant parameterization. To test this suggestion, it is necessary to scrutinize changes in the model performance.

To first gain a physical perspective of how the time-varying scheme directly affects the model, Figure 7 depicts the estimated large-scale vertical velocity at the top of the mixed layer (w_L). It is consistently negative, indicating net subsidence. By virtue of the scheme chosen, there is a large diurnal fluctuation, in accordance with the behavior of h(t). Without local subsidence velocity observations, however, this information alone cannot justify a net improvement.

As with the *nosub* versus *sub constant* case, tests of model performance are needed to make an appropriate comparison. Three tests are considered here: model error, convergence of solution and RMSE. As outlined in the experimental design description (Section 3.a), a time-varying subsidence parameterization should enhance

model physics to a greater extent than should a constant parameterization. Figures 8a and 8b show somewhat mixed results with respect to that postulate.

Figure 8a shows a negligible change ω_θ for the *sub* versus *sub constant* case with the greatest error reduction around the time of the frontal passage. Figure 8b, however, indicates a slight, but consistent error enhancement over the *sub constant* case. This result would suggest to the first order that the time-varying β_s approach fails over that of constant β_s. Given the incomplete understanding of the randon, time-varying model error variable, however, such a result is merely inconclusive. Additional tests are clearly needed to evaluate the performance of the *sub* case. For reference, Figure 8c depicts the evolution of $\omega_{\beta s}$. The lack of a diurnal signal in Figure 8c comparable to that seen in Figures 8a and 8b is evidence of the high decorrelation time scale, necessary for adequate numerical stability and physical relevance (see the covariance structure descriptions in Appendix C).

One method of evaluating the robustness of the time-varying β_s approach is to check for convergence of solution. A critical component of functionality for the *sub* case enhancement is the ability to properly diagnose the appropriate $\beta_s(t)$ evolution. Although the precise measurement of subsidence velocity in the atmosphere is quite sensitive, the enhancement should create a reasonably precise 'cone' of $\beta_s(t)$ from a systematic draw of β_{s_0} (such as in a simulation where β_{s_0} must be estimated from local observations). Figure 9 illustrates a limited such capability. From an initial range of 0.40×10^{-5} s^{-1}, the initial condition estimation procedure reduces the processing range to 0.28×10^{-5} s^{-1}, ultimately converging to a range of 0.24×10^{-5} s^{-1}. It should be noted, however, that the curves do favor the best convergence near the time of the frontal passage around day 154, with some slight evidence of divergence beyond that point. This feature may be indicative of a struggle to find convergence across two different synoptic regimes. Values of β_{s_0} up to and over 1×10^{-5} s^{-1} were tested thoroughly and found to diverge consistently. In light of the influence of the synoptic conditions, the degree to which the model converges seems appropriate as a mean estimate for a period with some cloud cover evident, given results from the literature (Table 1). One key shortcoming of

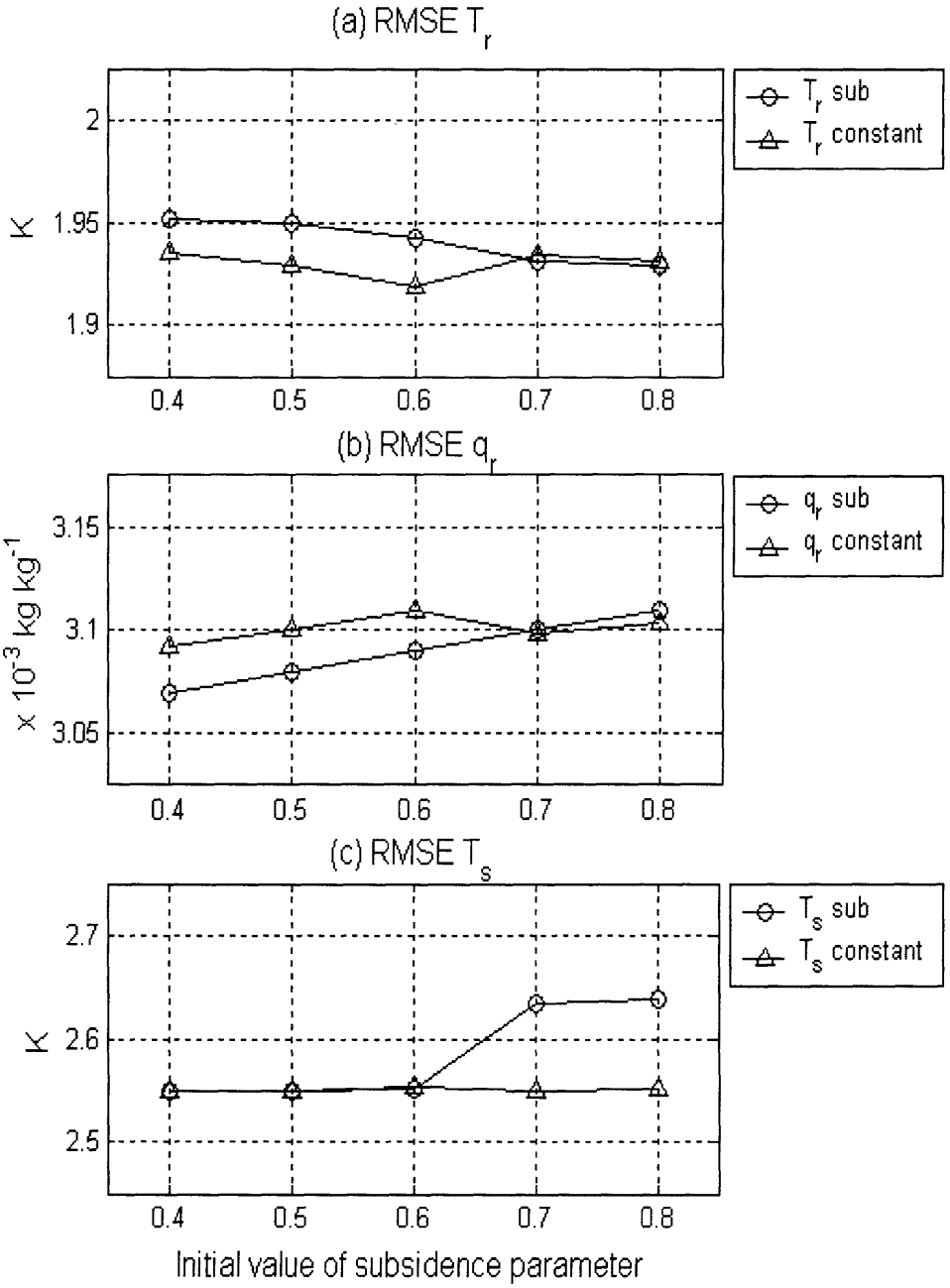

Figure 10: RMSE scores for T_r (a), q_r (b) and T_s (c) compared between a subsidence parameterization with a time-varying β_s (*sub*) and a constant β_s (constant). Scores for the constant parameterization are calculated from model results where β_s is maintained at a discrete value of β_{s_0} indicated by the open triangles. Scores for the time-varying parameterization are calculated from model results where β_s varies in time from its discrete value of β_{s_0}, indicated by open circles. Units of β_{s_0} along the abscissa are 10^{-5} s^{-1}.

this estimation, however, is the lack of response anticipated with respect to the synoptic conditions. One would expect an initially feeble subsidence to yield to a much more robust signal by day 155. However, this estimation result yields only a slight decrease in time, again, serving more as a period mean. This is likely due, in part, to the high decorrelation time set for this simulation (24 hours). This value was chosen to allow the model to reach a solution by reducing degrees of freedom as well as to smooth out any spurious divergence events. Though necessary physically, it may also unintentionally weaken the model's ability to respond quickly in the presence of a large divergence changes over a period of integration. It is likely that a dataset of much greater length would provide some improvement to the rate of convergence.

The final judge of model performance is the RMSE score test whose results can be seen in Figure 10. Scores were measured at the point of model convergence for the same series of discrete β_{s_0} depicted in Figure 9. Figure 10a shows consistently higher T_r RMSE due to the time-varying parameterization. Although the error gain is fairly negligible with respect to changes seen in Figure 6a (especially for the higher value β_{s_0} tests), the *nosub-sub constant* counterpart test, these results do suggest that the best model improvement for T_r rests with a constant β_s parameterization.

For the 2m specific humidity variable (q_r), there is a slight discrepancy of improvement with *sub* versus *sub constant* (Figure 10b). The lower end of the uncertainty cone produces clear net improvement, but this trend reverses for the β_{s_0} = 0.70 x 10^{-5} s^{-1} and 0.80 x 10^{-5} s^{-1} estimates. Thus, for the majority of the range of β_{s_0}, q_r is best solved by the time-varying scheme. In light of the dominant magnitude of ω_q versus ω_θ, as well as in the mixed layer fluxes, this is arguably a favorable result.

Once again, there is no improvement to T_s, seen in Figure 10c. No great improvement was anticipated for this measurement, as described above with reference to Figure 6. In general, the difference between *sub* and *sub constant* is negligible, except toward the higher β_{s_0} values. It is unclear why these particular values should contribute a net error gain.

Tests of model error reduction, parameter convergence and model performance improvement for the *sub* parameterization indicate mixed results. The random, time-

varying error parameter suggests a net gain of magnitude for ω_q. Yet, only q_r sustains any reasonable degree of consistent RMSE score reduction against the constant parameterization scheme. Clearly, the latter result is more robust. However, there is also a net gain of RMSE score error for T_r and the time-varying β_s is subject to fairly minimal convergence in time, weakening the case slightly. The latter shortcoming may be alleviated with model improvements and new, longer datasets. These initial results indicate the distinct potential for model improvement from a time-varying β_s parameterization, particularly with respect to the model moisture budget.

7. Future Directions and Study Limitations

This experiment demonstrates the potential for the resolution of a time-varying subsidence / divergence parameter in the ABL. The results here, however, do not confirm the ability to resolve subsidence. It is clear that without veritable measurements against which to compare the model estimates, the validity of these results remains in question. The next step, crucial to determining the viability of this approach, is to run a similar integration where reliable subsidence or large scale ABL divergence measurements are available, thus permitting a more complete assessment of model estimates. A successive study may involve using a similar dataset with this or any other one-dimensional ABL model. An alternative procedure could involve using a large-eddy simulation (LES) to derive a set of subsidence 'observations' against which one could compare model estimates with this or another one-dimensional ABL model.

If the viability of this subsidence estimation method were confirmed, additional testing would be necessary with multi-dimensional models that resolve advection. In such a case, the nature of the total model error would be vastly different and thus require new experiments to determine whether ω_{β_s} can estimate $\beta_s(t)$. These tests should also include cases of adverse meteorological conditions (within the limits to be expected by the model at hand) to confirm versatility. As discussed in Section 6b, possible shortcomings seen in the data, including a highly smoothed $\beta_s(t)$ curve, may be overcome with model improvements and longer datasets so as to avoid the numerical instability associated with shorter decorrelation time scales. Longer datasets will also permit the study of change across synoptic regimes. Although the results here do not indicate adequate resolution of such change, it may be permitted subject to a reduced decorrelation time scale.

8. CONCLUSION

This study examines the effect of large-scale ABL subsidence on model physics and model performance with the objective of evaluating an alternative method to account for this important physical process. Using a coupled land-ABL model with assimilated surface measurements, the first part of the study qualifies the net model improvement by a constant β_s parameterization (*sub constant*) over no subsidence parameterization (*nosub*). Model estimates confirm most physical changes anticipated from theory. These results indicate a small, but consistent reduction of model error. Model performance also improves, given the significant reduction of RMSE.

The second part of this study tests the ability to model a time-varying β_s. Model performance experiments yield conflicting results. The magnitude of model error changes little owing to the time-varying (*sub*) scheme (when compared against the *sub constant* approach), though there is a minor, consistent increase of $|\omega_q|$. RMSE score analysis reveals a net error increase for T_r, but a consistent decrease for q_r. The latter studies being the most robust of the comparative tests, these results suggest a favorable improvement for the moisture budget of the coupled model owing to the implementation of a time-varying β_s parameterization.

Evidence from the literature, confirmed by this study, demonstrates the need to account for subsidence in ABL modeling when meteorological conditions are favorable thereto. Given the frequently non-negligible influence of this phenomenon, it can be highly beneficial to have an accurate estimate. For multiple-day modeling of the ABL, the common constant β_s approach will not account for change in synoptic regime or any local effects, creating a potentially inaccurate parameterization. This study indicates the potential for improvement from a time-varying β_s approach. It is hoped that future investigations, perhaps with more complex models and data assimilation schemes, will consider adopting the time-varying β_s approach to alleviate unknown model error and improve model performance in the ABL.

REFERENCES:

Batchvarova, E. and S. Gryning. 1994. An Applied Model for the Height of the Daytime Mixed Layer and the Entrainment Zone. *Boundary Layer Meteorology*. **71**, 311-323.

Batchvarova, E. and X. Cai and S. Gryning and D. Steyn. 1999. Modelling Internal Boundary-Layer Development in a Region with a Complex Coastline. *Boundary Layer Meteorology*. **90**, 1-20.

Batchvarova, E. and S. Gryning and C. Hasager. 2001. Regional Fluxes of Momentum and Sensible Heat over a Sub-Arctic Landscape During Late Winter. *Boundary Layer Meteorology*. **99**, 489-507.

Betts, A. 2000. Idealized Model for Equilibrium Boundary Layer over Land. *Journal of Hydrometeorology*. **1**, 507-523.

Betts, A. and J. Ball. 1998. FIFE surface climate and site-averaged dataset 1987-1989. *Journal of the Atmospheric Sciences*. **55**, 1091-1108.

Carlson, Merrilee A. and R. Stull. 1986. Subsidence in the Nocturnal Boundary Layer. *Journal of Climate and Applied Meteorology*. **25**, 1088-1099.

Deardorff, J. and E. Peterson. 1980. The Boundary-Layer Growth Equation with Reynolds Averaging. *Journal of the Atmospheric Sciences – Notes and Correspondence*. **37**, 1405-1410.

de Arellano, J. and B. Gioli and F. Miglietta and H. Jonker and H. Baltink and R. Hutjes and A. Holtslag. 2004. Entrainment process of carbon dioxide in the atmospheric boundary layer. *Journal of Geophysical Research – Atmospheres*. **109** (D18). D18110.

De Ridder, K. 1997. Land Surface Processes and the Potential for Convective Precipitation. *Journal of Geophysical Research.* **102** (D25), 30085-30090.

De Wekker, S. and D. Steyn and S. Nyeki. 2004. A comparison of aerosol-layer and convective boundary-layer structure over a mountain range during Staaarte '97. *Boundary Layer Meteorology.* **113**, 249-271.

Driedonks, A. 1982. Models and Observations of the Growth of the Atmospheric Boundary Layer. *Boundary Layer Meteorology.* **23**, 283-306.

Driedonks, A. and H. Tennekes. 1984. Entrainment Effects in the Well-Mixed Atmospheric Boundary Layer. *Boundary Layer Meteorology.* **30**, 75-105.

Ek, M. and L. Mahrt. 1994. Daytime Evolution of Relative Humidity at the Boundary Layer Top. *Monthly Weather Review.* **122**, 2709-2721.

Fitzjarrald, D. 1982. New Applications of a Simple Mixed Layer Model. *Boundary Layer Meteorology.* **22**, 431-451.

Kirkpatrick, M. and N. Mansour and A. Ackerman and D. Stevens. 2003. Dynamic turbulence modeling in large-eddy simulations of the cloud-topped atmospheric boundary layer. *Center for Turbulence Research Annual Research Briefs 2003.* 23-37.

Letzel, M. and S. Raasch. 2002. Large-Eddy Simulations of Thermally Induced Oscillations in the Convective Boundary Layer. *Annual Journal of Hydraulic Engineering.* **46**, 67-72.

Margulis, S. 2002. Variational Sensitivity Analysis and Data Assimilation Studies of the Coupled Land Surface-Atmospheric Boundary Layer System. PhD. Thesis, Massachusetts Institute of Technology, 205 pp.

Margulis, S. and D. Entekhabi. 2001. A Coupled Land Surface-Boundary Layer Model and its Adjoint. *Journal of Hydrometeorology*. **2**, 274-296.

Margulis, S. and D. Entekhabi. 2003. Variational Assimilation of Radiometric Surface Temperature and Reference-Level Micrometeorology into a Model of the Atmospheric Boundary Layer and Land Surface. *Monthly Weather Review*. **131**, 1272-1288.

Margulis, S. and D. Entekhabi, 2004. Boundary-Layer Entrainment Estimation Through Assimilation of Radiosonde and Micrometeorological Data into a Mixed-Layer Model. *Boundary Layer Meteorology*. **110**, 405-433.

McNaughton, K. and T. Spriggs. 1986. A Mixed-Layer Model for Regional Evaporation. *Boundary Layer Meteorology*. **34**, 243-262.

Press, W. and S. Teukolsky and W. Vetterling and B. Flannery. 1989. Numerical Recipes: The art of scientific computing. Cambridge University Press: Cambridge. 702 pp.

Price, H. and D. Jaffe and O. Cooper and P. Doskey. 2004. Photochemistry, ozone production, and dilution during long-range transport episodes from Eurasia to the northwest United States. *Journal of Geophysical Research-Atmospheres*. **109** (D23), D23S13.

Reichle, R. 2000. Variational assimilation of remote sensing data for land surface hydrological applications. PhD. Thesis, Massachusetts Institute of Technology, 192 pp.

Sellers, P. and F. Hall and G. Asrar and D. Strebel and R. Murphy. 1992. An overview of the first international satellite land surface climatology project (ISLSCP) field experiment (FIFE). *Journal of Geophysical Research*. **97** (D17), 18345-18371.

Sempreviva, A. and S. Gryning. 2000. Mixing Height Over Water and its Role on the Correlation Between Temperature and Humidity Fluctuations in the Unstable Surface Layer. *Boundary Layer Meteorology*. **97**, 273-291.

Sorbjan, Z. 1995. Toward Evaluation of Heat Fluxes in the Convective Boundary Layer. *Journal of Applied Meteorology*. **34**, 1092-1098.

Stevens, B. and A. Ackerman and B. Albrecht and A. Brown and M. Macvean and A. Chlond and J. Cuxart and E. Sánchez and P. Duynkerke and D. Lewellen and R. Neggers and A. Siebesma and D. Stevens. 2001. Simulations of Trade Wind Cumuli under a Strong Inversion. *Journal of the Atmospheric Sciences*. **58**, 1870-1891.

Steyn, D. and T. Oke. 1982. The Depth of the Daytime Mixed Layer at Two Coastal Sites: A Model and its Validation. *Boundary Layer Meteorology*. **24**, 161-180.

Stull, R. 1973. Inversion Rise Model Based on Penetrative Convection. *Journal of the Atmospheric Sciences*. **30**, 1092-1099.

Stull, R. 1976. Mixed-Layer Depth Model Based on Turbulent Energetics. *Journal of the Atmospheric Sciences*. **33**, 1268-1278.

Stull, R. 1988. An Introduction to Boundary Layer Meteorology. Kluwer Academic Publishers: Dordrecht. 670 pp.

Yi, C. and K. Davis and B. Berger. 2001. Long-Term Observations of the Dynamics of the Continental Planetary Boundary Layer. *Journal of Atmospheric Sciences*. **58**, 1288-1299.

ACKNOWLEDGEMENTS

I extend great thanks to my advisor, Professor Dara Entekhabi, for his guidance throughout the course of my research on this project. He consistently offered fresh, valuable perspective and also provided me with insightful academic counsel throughout my years at M.I.T. I also extend my thanks to Professor R. Alan Plumb, advisor for my first semesters of graduate study at M.I.T. and mentor in the balance of my studies.

I also wish to thank those who contributed to my study through discussion of important issues in data assimilation and adjoint models: Professor Steven Margulis, Ian Fenty and Jonathan Moskaitis. A special thank you to all the students, staff, post-docs, research scholars and faculty of the Program in Atmospheres, Oceans and Climate (PAOC). Each of you made a unique contribution to my life at M.I.T. and I am very grateful to have worked with all of you.

Finally, I wish to thank my family, my mother, my father and my brother Steven, for their steadfast support throughout my coursework and research. They provided sincere encouragement and a keen perspective on my goals and aspirations.

APPENDIX A: LIST OF SYMBOLS

Label	Description	Units or [Dimension]
b	Large-scale ABL divergence from Stull (1973)	s^{-1}
$\mathbf{C}_\beta$	Prior initial condition error covariance	
C_c	Canopy heat capacity	J m^{-2} K^{-1}
C_d	Deep soil heat capacity	J m^{-2} K^{-1}
C_g	Surface soil heat capacity	J m^{-2} K^{-1}
c_h	ABL growth proportionality constant	
C_v	Measurement error covariance	
c_p	Dry air specific heat	J kg^{-1} K^{-1}
$\mathbf{C}_\omega(t,t')$	Prior model error covariance	
d1	Thickness of soil layer 1	m
d2	Thickness of soil layer 2	m
d3	Thickness of soil layer 3	m
E_c	Transpiration from canopy	kg m^{-2} s^{-1}
E_{c1}	Transpiration taken from soil layer 1	kg m^{-2} s^{-1}
E_{c2}	Transpiration taken from soil layer 2	kg m^{-2} s^{-1}
E_g	Evaporation from ground	kg m^{-2} s^{-1}
e	Atmospheric vapor pressure	Pa
$e_s(T)$	Atmospheric saturation vapor pressure at temperature T	Pa
E_{top}	Dry air entrainment	kg m^{-2} s^{-1}
$f(\mathbf{y},\alpha)$	Nonlinear function of state variables and parameters	
$\mathbf{F}$	Nonlinear operator	
$g(\mathbf{y})$	Generic function to be minimized by Lagrangian	
$\mathbf{g}$	Gravitational acceleration	ms^{-2}
G_*	Production of mechanical turbulent energy	m^3 s^{-3}

Label	Description	Units or [Dimension]
$[\delta]$	Diagonal matrix of Dirac delta functions with respect to observation times	
Δt	Numerical model timestep	s
α	Vector of time-varying model parameters	
β	Random, time-invariant error parameter	
β_s	Subsidence parameter	s^{-1}
δ_θ	Inversion strength of θ	K
δ_q	Inversion strength of q	kg kg^{-1}
ε	Scalar step size	
ε_a	Mixed-layer bulk emissivity	
γ_θ	Lapse rate of θ above h	K m^{-1}
γ_q	Lapse rate of q above h	kg kg^{-1} m^{-1}
η_β	Ratio of ε to $\mathbf{C}_\beta$	
η_ω	Ratio of ε to $\mathbf{C}_\omega$	
λ	Adjoint variable / Lagrange multiplier	
λ_h	Adjoint variable for h	
$\lambda_{\beta s}$	Adjoint variable for β_s	
θ	Potential Temperature	K
θ_s	Soil porosity	
ρ	Air density	kg m^{-3}
ρ'	Eddy fluctuation of air density	kg m^{-3}
$\phi(\mathbf{x})$	Function constraint in Lagrangian	
ρ_w	Density of water	kg m^{-3}
σ^2_β	Random, time-invariant error variance	
σ^2_ω	Model error variance	[y^2 t^{-2}]

h	Mixed layer depth	m
H_c	Sensible heat flux from canopy	W m^{-2}
H_g	Sensible heat flux from ground	W m^{-2}
H_{top}	Sensible heat flux entrainment	W m^{-2}
H_v	Virtual heat flux	W m^{-2}
J	Model response functional	
J'	Objective function / Performance index	
k	iteration number	
L_v	Latent heat of vaporization	J kg^{-1}
$\mathbf{M}$	Model measurement vector operator	[**Z** y^{-1}]
p	Air pressure	Pa
p'	Eddy fluctuation of air pressure	Pa
P_{w1}	Moisture infiltration into soil layer 1	m s-1
q	Mixed layer specific humidity	kg kg^{-1}
$Q_{1,2}$	Flow between soil layers 1 and 2	m s^{-1}
$Q_{2,3}$	Flow between soil layers 2 and 3	m s^{-1}
Q_3	Gravitational drainage from layer 3	m s^{-1}
q_r	Reference level specific humidity	kg kg^{-1}
R_{ad}	Downwelling longwave radiation from above the mixed layer	W m^{-2}
R_{Ad}	Downwelling longwave radiation from within the mixed layer	W m^{-2}
R_{Au}	Upwelling longwave radiation from within the mixed layer	W m^{-2}
R_{cu}	Upwelling longwave radiation from the canopy into the mixed layer	W m^{-2}
R_{gu}	Upwelling longwave radiation from the ground into the mixed layer	W m^{-2}
RMSE	Root-mean-square error	

τ	Decorrelation time scales	
τ_a	Annual period days	
τ_d	Diurnal period	s-1
$\boldsymbol{\omega}$	Model error parameter	[**y** t^{-1}]
$\omega_{\beta s}$	Model error for β_s	[s^{-1} t^{-1}]
ω_θ	Model error for θ	[K t^{-1}]
ω_q	Model error for q	[kg kg^{-1} t^{-1}]
ξ	Mechanical turbulence dissipation parameter	m^{-1}
$\bar{\beta}$	Prior estimate of random, time-invariant error	
$\bar{\omega}$	Prior estimate of model error	[**y** t^{-1}]
ν_m	Kinematic molecular viscosity	m^2 s^{-1}
$\boldsymbol{\nu}$	Measurement error vector	[**Z**]

R_{nc}	Net radiation absorbed by the canopy	W m^{-2}
R_{ng}	Net radiation absorbed by the ground	W m^{-2}
t	Time	s
T_c	Canopy temperature	K
T_d	Deep soil temperature	K
T_g	Ground temperature	K
T_r	Reference level temperature	K
T_s	Radiometric surface temperature	K
u	Mean ABL eastward wind component	m s^{-1}
u_p	Generic parameter	
v	Mean ABL northward wind component	m s^{-1}
$\overline{w}$	Linearly averaged vertical velocity	m s^{-1}
w'	Eddy fluctuation of vertical velocity	m s^{-1}
w_e	Entrainment velocity	m s^{-1}
W_1	Layer-1 soil saturation	
W_2	Layer-2 soil saturation	
W_3	Layer-3 soil saturation	
w_L, w_s	Subsidence velocity	m s^{-1}
$\mathbf{y}(t)$	State variable	
$\mathbf{Z}$	Assimilated measurement	

APPENDIX B: LAND SURFACE PROGNOSTIC EQUATIONS

Surface energy budget equations:

$$C_c \frac{dT_c}{dt} = R_{nc} - H_c - L_v E_c \tag{A1}$$

$$C_g \frac{dT_g}{dt} = (R_{ng} - H_g - L_v E_g) - \frac{2\pi C_d}{\tau_d}(T_g - T_d) \tag{A2}$$

$$C_d \frac{dT_d}{dt} = \frac{1}{2(\pi\tau_a)^{1/2}}\left(R_{ng} - H_g - L_v E_g\right) \tag{A3}$$

Surface moisture budget equations:

$$\frac{dW_1}{dt} = \frac{1}{\theta_s d_1}\left(P_{w1} - Q_{1,2} - \frac{1}{\rho_w}E_g - \frac{1}{\rho_w}E_{c1}\right) \tag{A4}$$

$$\frac{dW_2}{dt} = \frac{1}{\theta_s d_2}\left(Q_{1,2} - Q_{2,3} - \frac{1}{\rho_w}E_{c2}\right) \tag{A5}$$

$$\frac{dW_3}{dt} = \frac{1}{\theta_s d_3}\left(Q_{2,3} - Q_3\right) \tag{A6}$$

APPENDIX C: COVARIANCE STRUCTURES

a) Model Error Covariance ($\mathbf{C}_\omega$)

i. Design

The unknown, time-varying model error, ω, is calculated iteratively by equation (26). As described in section 4, the model error is meant to represent the sum of effects from all physical processes unaccounted for in the solution of each state variable. The error can exist in each forward model prognostic equation (4-10, 14). In this study, however, the one-dimensional model is assumed to incur the majority of model error due to the neglect of advection. Thus, ω is solved only for those variables believed to sustain a large error (with respect to ambient variations, such as diurnal fluctuation) caused by advection: θ, q and β_s.

At each iterative update in (26), for $\mathbf{y} = \{\theta, q, \beta_s\}$ the error, ω_y, derives from the convolution of the adjoint variable λ_y and an appropriate covariance $C_{\omega y}(t,t')$. The covariance factor allows model imperfection, conceived through the adjoint variable, to be mapped back into the forward model. It does this by reducing the degrees of freedom of the model error (to permit solution) and applying an appropriate magnitude (error variance) to the error structure. Although the model error is presumed to derive from advection, the error structure itself is unknown. In such a situation, an appropriate structure for $C_{\omega y}$ (Margulis 2002, Reichle 2000) is described by:

$$\mathbf{C}_{\omega_y}(t,t') = \sigma^2_{\omega_y} \mathbf{exp}\left(\frac{|t-t'|}{\tau}\right) \qquad \text{(A7)},$$

where $\sigma^2_{\omega y}$ is the model error variance (units of $\frac{[y]^2}{[t]^2}$) and τ is the model error decorrelation time scale.

ii. Variance (σ^2_ω)

The variance for the three state variables is set to account for reasonable variation in time by advection. For θ and q, this means a flux, estimated to be around 20 Wm^{-2}. The parameter β_s is more sensitive. Without knowledge a priori of the subsidence evolution in time, this variance must be estimated so as to permit the optimal solution of $\beta_s(t)$ and is set to change according to the magnitude of $\beta_s(t)$: $1x\ 10^{-16}\ |\beta_{s_0}|$, constant throughout each iteration.

iii. Decorrelation Time Scale (τ)

Mathematically, τ is a smoothing time scale for the correlation function $\left(\mathbf{exp}\left(\frac{|t-t'|}{\tau}\right)\right)$. By smoothing the adjoint variables, it acts to reduce the number of unknowns present in the model error, thus permitting estimation. It does this numerically by assigning a relatively high correlation among temporally adjacent, discrete model

error values. From a physical perspective, τ is an isotropic correlation time scale. Its numerical form represents, roughly, the time scale over which the missing processes are correlated. In light of the sensitive, but slowly varying nature of subsidence and the need to reduce model error degrees of freedom, $\tau_{\omega_{\beta_s}}$ is set to 24 hours. Based on typical advection time scales, τ_{ω_θ} and τ_{ω_q} are set to six hours.

iv. *Numerical considerations*

The numerical solution of the analytical model error functions present two areas in need of adaptation. The process of convolution follows the signal-response example described by Press et al. (1989). This numerical procedure necessitates a cut-off point for the correlation function (e.g., a limit of correlation strength by which two discrete adjoint variable solutions are correlated in the creation of the model error). This value is set 0.15, to permit some high-frequency variation in model error, minimize undesirable inflation of model error and minimize unknowns. An additional numerical issue arises because λ_f=0. This boundary condition serves to bias the evolution of λ from t_f to t_0. To avoid this and further complications from the convolution method, a damped, reflective boundary condition is installed beyond the signal boundaries (t_0, t_f) to assuage the zero-bias.

b) *Initial Condition Error Covariance ($\mathbf{C}_\beta$)*

An initial condition error covariance is defined for the estimation of initial values for the state variables believed to have a longer memory and, thus, better estimation ability through data assimilation (ME03). The variables W_{1_0}, W_{2_0}, θ_0, q_0 and β_{s_0} are selected for estimation. The initial condition error, $\boldsymbol{\beta}$, is random, but unlike $\boldsymbol{\omega}$, it is not time-varying. Its covariance is defined as a diagonal matrix with error standard deviations (σ_β) of 20 percent for W_{1_0}, W_{2_0}, β_{s_0}, 2 K for θ_0 and 2 g kg^{-1} for q_0. Equation 25 incorporates $\mathbf{C}_\beta$ into the solution for $\boldsymbol{\beta}$.

c) *Measurement Error Covariance ($\mathbf{C}_v$)*

Measurement error is assumed to be unbiased and uncorrelated in the model. As such, $\mathbf{C}_v$ is specified to reflect commonly used model error standard deviations. The measurements assimilated into the model in this study are T_r, q_r and T_s. Each measurement has a corresponding measurement error standard deviation of 0.5 K, 0.5 g kg^{-1} and 0.5 K, respectively (ME03).